

5-2014

A Numerical Model for Nonadiabatic Transitions in Molecules

Devanshu Agrawal

Follow this and additional works at: <http://dc.etsu.edu/honors>

 Part of the [Applied Mathematics Commons](#), [Mathematics Commons](#), and the [Physics Commons](#)

Recommended Citation

Agrawal, Devanshu, "A Numerical Model for Nonadiabatic Transitions in Molecules" (2014). *Undergraduate Honors Theses*. Paper 193.
<http://dc.etsu.edu/honors/193>

This Honors Thesis - Open Access is brought to you for free and open access by Digital Commons @ East Tennessee State University. It has been accepted for inclusion in Undergraduate Honors Theses by an authorized administrator of Digital Commons @ East Tennessee State University. For more information, please contact digilib@etsu.edu.

A Numerical Model for Nonadiabatic Transitions in Molecules

A thesis

presented to

the faculty of the Departments of Mathematics and of Physics

East Tennessee State University

In partial fulfillment

of the requirements for the degree

Bachelor of Science in Mathematics and Physics with Honors

by

Devanshu Agrawal

April 2014

Frank Hagelberg, Ph.D., Chair

Jeff Knisley, Ph.D.

Mark Giroux, Ph.D.

Copyright by Devanshu Agrawal 2014

DEDICATION

I would like to dedicate my thesis to my high school vision education teacher, Mrs. Nila Collins. Without the skills she taught me and the support she gave me while I was losing my vision during high school, I could not have come so far.

I would also like to dedicate this thesis to my high school calculus teacher, Mr. Guy Mauldin. He is the man who encouraged me to pursue mathematics and physics despite my disability and sparked in me a passion for the subjects.

ACKNOWLEDGMENTS

First and foremost, I would like to thank my thesis advisor Dr. Frank Hagelberg for his guidance and support throughout this project. I want to thank him for sparking my interest in quantum mechanics in the classroom, for introducing me to the world of numerical programming (and his patience with me as I learned), and for continuously challenging me with new scenarios that allowed this project to evolve. This project has been an excellent experience, and I am very grateful to Dr. Hagelberg for making it possible.

I would also like to thank Dr. Jeff Knisley for helping me with the LaTeX code used to produce this document. Without his support, it would have taken much longer to get the thesis in its final form. Additionally, I want to thank everyone in the Department of Mathematics, Department of Physics, and the Honors College who was involved in my college education.

Finally, special thanks to my friends and family for their support and significant help throughout my college experience. I could not have done it without them.

ABSTRACT

In molecules, electronic state transitions can occur via quantum coupling of the states. If the coupling is due to the kinetic energy of the molecular nuclei, then electronic transitions are best represented in the adiabatic frame. If the coupling is instead facilitated through the potential energy of the nuclei, then electronic transitions are better represented in the diabatic frame. In our study, we modeled these latter transitions, called “nonadiabatic transitions.” For one nuclear degree of freedom, we modeled the de-excitation of a diatomic molecule. For two nuclear degrees of freedom, we modeled the de-excitation of an ethane-like molecule undergoing cis-trans isomerization. For both cases, we studied the dependence of the de-excitation on the nuclear configuration and potential energy of the molecule.

We constructed a numerical model to solve the time-dependent Schrödinger Equation for two coupled wave functions. Our algorithm takes full advantage of the sparseness of the numerical system, leading to a final set of equations that is solved recursively using nothing more than the Tridiagonal Algorithm.

We observed that the most effective de-excitation occurred when the molecule transitioned from a stable equilibrium configuration to an unstable equilibrium configuration. This same mechanism is known to drive fast electronic transitions in the adiabatic frame. We concluded that while the adiabatic and diabatic frames are strongly opposed physically, the mathematical mechanism driving electronic transitions in the two frames is in some sense the same.

CONTENTS

| | |
|---|----|
| LIST OF TABLES | 7 |
| LIST OF FIGURES | 9 |
| 1 Introduction | 10 |
| 1.1 The Adiabatic and Diabatic Frames | 12 |
| 1.2 The One-Dimensional Single-State Case | 17 |
| 1.3 The One-Dimensional Two-State Case | 19 |
| 1.4 The Two-Dimensional Two-State Case | 21 |
| 2 Methodology | 26 |
| 2.1 The One-Dimensional Single-State Case | 26 |
| 2.2 The One-Dimensional Two-State Case | 29 |
| 2.3 The Two-Dimensional Two-State Case | 32 |
| 2.4 Normalization and Expectation Values | 35 |
| 2.4.1 In One Dimension | 35 |
| 2.4.2 In Two Dimensions | 37 |
| 3 Results | 40 |
| 3.1 The One-Dimensional Single-State Case | 40 |
| 3.2 The One-Dimensional Two-State Case | 41 |
| 3.3 The Two-Dimensional Two-State Case | 46 |
| 4 Discussion | 59 |
| 5 Future Work | 64 |
| BIBLIOGRAPHY | 65 |

LIST OF TABLES

| | | |
|---|---|----|
| 1 | List of the model parameter values used for each case of Phase 2. . . | 42 |
| 2 | List of the model parameter values used for each case in Phase 3. . . | 46 |

LIST OF FIGURES

| | | |
|----|---|----|
| 1 | Plot of the Morse PE function $V(X)$. The horizontal asymptote of $V(X)$ is the dissociation energy E_d | 20 |
| 2 | Plots of the Morse potential $V_1(X)$, the repelling potential $V_2(X)$, and the coupling potential $V_{12}(X)$ for the case $(A, B, C, D, E) = (10, 20, 10, 0.1, 0)$ | 22 |
| 3 | Plots of some sectional curves of the PE functions. | 25 |
| 4 | Plots of expectation values for both cases considered in Phase 1. | 51 |
| 5 | Plots of the ground state population and the force expectation value against time for Case 1 (the standard case) in Phase 2. | 52 |
| 6 | Plots of the ground state population against time for two different values of the parameter B in Phase 2. The standard value is $B = 20$ used in Case 1 (Figure (4a)). | 53 |
| 7 | Plots of the ground state population against time for two different values of the parameter C in Phase 2. The standard value is $C = 15$ used in Case 1 (Figure (4a)). | 53 |
| 8 | Plots of the ground state population against time for two different values of the parameter D in Phase 2. The standard value is $D = 0.1$ used in Case 1 (Figure (4a)). | 54 |
| 9 | Plots of the ground state population against time for two different values of the parameter E in Phase 2. The standard value is $E = 0$ used in Case 1 (Figure (4a)). | 54 |
| 10 | Plots of the torsion angle, ground state population, and torque for a molecule in Case 1 of Phase 3. | 55 |

| | | |
|----|--|----|
| 11 | Plots of the torsion angle, ground state population, and torque for a molecule in Case 2 of Phase 3. | 56 |
| 12 | Plots of the torsion angle, ground state population, and torque for a molecule in Case 3 of Phase 3. | 57 |
| 13 | Plots of the torsion angle, ground state population, and torque for a molecule in Case 4 of Phase 3. | 58 |

1 Introduction

Molecular physics as a subject studies the structure and the dynamics of molecules. The positions of the atomic nuclei comprising the molecule relative to one another defines a “nuclear configuration” that specifies a shape for the molecule. We are concerned with the physical laws that dictate the evolution of this shape with time.

In physics, motion is often determined by a “potential energy surface.” For a molecule, we can associate with every nuclear configuration a potential energy. In this way, a potential energy (PE) surface is defined over the nuclear configuration space. But let us also note that for any nuclear configuration, there are infinitely many ways that the electrons surrounding the nuclei can be configured. In particular, a discrete or “quantized” set of possible electronic configurations or “states” accompanies every possible nuclear configuration. Each electronic state has its own characteristic energy; the lowest-energy state is called the ground state, the second-lowest-energy state is called the first excited state, and so on. It follows that not one but an infinite set of potential energies is associated to every nuclear configuration. In this way, the internal, or nuclear, motion of a molecule is guided not by one but rather an infinite set of PE surfaces— one for every electronic state. This infinite family of PE surfaces is called a potential energy (PE) landscape.

The configuration of a molecule is given by a quantum state function or “wave function,” whose square magnitude gives the probability density for observing the molecule to have a particular configuration. The wave function evolves in the PE landscape of the molecule. Under certain assumptions, it is possible to split the wave function so that for every surface in the PE landscape, some fraction of the wave

function evolves on that surface. These fractions of the wave function, however, do not evolve independently. More generally, it is possible to study the evolution of a molecule on a single PE surface if we assume that the electrons of the molecule occupy a single, fixed electronic state. But in reality, it is possible for a wave function to transition from one surface to another, thanks to the quantum coupling of states via nuclear kinetic energy and potential energy. Therefore, the distribution of the wave function over the surfaces in the landscape changes with time. When a wave function transitions from one surface to another in this way, it is called an “electronic state transition.” When most of the wave function lies on the lowest surface in the landscape, then it is most probable that the electrons of the molecule will be observed in the ground state. In this case, we say that the molecule is in the ground state. Otherwise, the molecule is excited.

An electronic state transition can occur if the molecule radiates energy. Such a transition does not directly depend on the PE landscape itself; such a transition can happen at any nuclear configuration. Non-radiative transitions are more interesting. Such a transition occurs due to quantum coupling, as described above. Non-radiative transitions are interesting because their probability depends on the geometry or “shape” of the PE landscape. They are more likely at some nuclear configurations than at others. Therefore, the shape of the PE landscape governs both the shape of the molecule as well as its electronic energy. Since the internal motion of a molecule is faster on a lower surface (by conservation of energy), it follows that the speed of internal motion is related to the shape of the molecule. In fact, there are often special points in a PE landscape that act as “funnels” through which a

wave function can transition very quickly; these points are optimal configurations for fast state transitions. These “funnels” are actually points at which two PE surfaces intersect. Such a topology commonly characterizes the PE landscapes of biological molecules that must quickly transition to the ground state in order to maintain homeostasis. More generally, understanding molecular dynamics in the setting of a PE landscape is foundational to a strong theoretical understanding of chemistry as a whole. In our study, we are interested in the dependence of internal motion and state transitions on the shape of the PE landscape of a molecule [1].

1.1 The Adiabatic and Diabatic Frames

Consider any polyatomic molecule, and let \mathbf{x}_i and \mathbf{X}_j be the positions of the i th electron and j th nucleus respectively. Let \mathbf{x} be the list of the electron positions and \mathbf{X} the list of nuclear positions. Then, we denote the molecular wave function at time t as $\Psi(\mathbf{x}, \mathbf{X}, t)$. The molecular wave function evolves according to the time-dependent Schrödinger Equation:

$$i\hbar \frac{\partial}{\partial t} \Psi(\mathbf{x}, \mathbf{X}, t) = [\hat{\mathbf{T}}_N(\mathbf{X}) + U_N(\mathbf{X}) + \hat{\mathbf{H}}_e(\mathbf{x}, \mathbf{X})] \Psi(\mathbf{x}, \mathbf{X}, t), \quad (1)$$

where $\hat{\mathbf{T}}_N$ is the total nuclear kinetic energy (KE) operator, U_N is the nuclear potential energy (PE) function due to nucleus-nucleus repulsion, and $\hat{\mathbf{H}}_e$ is the electronic part of the molecular Hamiltonian. The nuclear KE operator is given by

$$\hat{\mathbf{T}}_N(\mathbf{X}) = \sum_i -\frac{\hbar^2}{2M_i} \frac{\partial^2}{\partial X_i^2},$$

where M_i is the mass of the i th nucleus and $\frac{\partial^k}{\partial X_i^k}$ denotes the sum of the k th derivatives with respect to the components of \mathbf{X}_i . The electronic Hamiltonian is given by

$$\hat{\mathbf{H}}_e(\mathbf{x}, \mathbf{X}) = \hat{\mathbf{T}}_e(\mathbf{x}) + U_e(\mathbf{x}) + U_{e,N}(\mathbf{x}, \mathbf{X}),$$

where $\hat{\mathbf{T}}_e$ is the total electronic KE operator, U_e is the PE function due to electron repulsion, and $U_{e,N}$ is the PE function due to electron-nucleus attraction. We are primarily interested in the evolution of the shape (or nuclear configuration) of the molecule and would therefore like an evolution equation for the nuclear part of the molecular wave function. It is possible to simplify Equation (1) by assuming that the electrons occupy an energy eigenstate. This simplification can be made in one of two settings– the adiabatic frame, and the nonadiabatic (or diabatic) frame.

For the adiabatic frame, let $\psi_n(\mathbf{x}, \mathbf{X})$ be the n th electronic energy eigenstate given that the nuclei have configuration \mathbf{X} . Note that the nuclear configuration \mathbf{X} is treated as a parameter in ψ_n . Thus, the energy eigenvalue E_n associated with ψ_n is a function of \mathbf{X} :

$$E_n(\mathbf{X}) = \langle \psi_n(\mathbf{x}, \mathbf{X}) | \hat{\mathbf{H}}_e(\mathbf{x}, \mathbf{X}) | \psi_n(\mathbf{x}, \mathbf{X}) \rangle,$$

where the bracket is taken over \mathbf{x} . The set of eigenfunctions $\{\psi_n\}$ forms a basis (or frame) for the space of molecular wave functions. In particular, we can write

$$\Psi(\mathbf{x}, \mathbf{X}, t) = \sum_n \chi_n(\mathbf{X}, t) \psi_n(\mathbf{x}, \mathbf{X}), \quad (2)$$

where χ_n is the nuclear wave function given that the electrons occupy the n th electronic energy eigenstate. Substituting Equation (2) into Equation (1) and simplifying, we obtain an evolution for the m th nuclear wave function χ_m in the adiabatic frame:

$$i\hbar \frac{\partial}{\partial t} \chi_m(\mathbf{X}, t) = (\hat{\mathbf{T}}_N + U_N + E_m)(\mathbf{X}) \chi_m(\mathbf{X}, t) + \sum_n L_{mn}(\mathbf{X}) \chi_n(\mathbf{X}, t), \quad (3)$$

where L is the non-adiabaticity matrix with entries

$$L_{mn} = \sum_i -\frac{\hbar^2}{2M_i} \left(2\langle\psi_m|\frac{\partial}{\partial X_i}|\psi_n\rangle\frac{\partial}{\partial X_i} - \langle\psi_m|\frac{\partial^2}{\partial X_i^2}|\psi_n\rangle \right). \quad (4)$$

Let $V_m^A(\mathbf{X}) = (U_N + E_m)(\mathbf{X})$. This is called the m th adiabatic PE surface, and it acts as an effective PE function for the nuclear wave function. The set of all adiabatic PE surfaces is called the adiabatic PE landscape. In addition to the nuclear KE operator and effective PE function, Equation (3) includes additional derivative coupling terms given by the off-diagonal entries of L .

For the diabatic frame, we assume the stronger condition that the electronic eigenstates are in some sense independent of the nuclear configuration. Choose any particular nuclear configuration \mathbf{X}^0 and let $\phi_n(\mathbf{x}) = \psi_n(\mathbf{x}, \mathbf{X}^0)$ for all n . The set of eigenfunctions $\{\phi_n\}$ also forms a basis (or frame) for the space of all molecular wave functions. In particular, we can write

$$\Psi(\mathbf{x}, \mathbf{X}, t) = \sum_n \chi_n(\mathbf{X}, t)\phi_n(\mathbf{x}), \quad (5)$$

where χ_n is the nuclear wave function given that the electrons occupy the n th energy eigenstate. Given that the ϕ_n are orthonormal and Ψ is normalized, the probability for observing the molecule in the n th electronic eigenstate is $\langle\chi_n(\mathbf{X})|\chi_n(\mathbf{X})\rangle$. This implies the identity

$$\sum_n \langle\chi_n|\chi_n\rangle = 1. \quad (6)$$

Substituting Equation (5) into Equation (1) and simplifying, we obtain an evolution equation for the m th nuclear wave function χ_m in the diabatic frame:

$$i\hbar\frac{\partial}{\partial t}\chi_m(\mathbf{X}, t) = \hat{\mathbf{T}}_N\chi_m(\mathbf{X}, t) + \sum_n V_{mn}^D(\mathbf{X})\chi_n(\mathbf{X}, t), \quad (7)$$

where V^D is the diabatic PE matrix with entries

$$V_{mn}^D(\mathbf{X}) = V_m^A(\mathbf{X}^0) + \langle \phi_m(\mathbf{x}) | [U_N(\mathbf{X}) + U_{e,N}(\mathbf{x}, \mathbf{X}) - U_N(\mathbf{X}^0) - U_{e,N}(\mathbf{x}, \mathbf{X}^0)] | \phi_n(\mathbf{x}) \rangle. \quad (8)$$

The diagonal entries V_{mm}^D are called diabatic PE surfaces. The set of all diabatic PE surfaces is called the diabatic PE landscape. The off-diagonal terms are the diabatic coupling PE terms. Since the operator in brackets in Equation (8) is a scalar function, the brackets are symmetric with respect to the indices m and n . That is, the PE matrix V^D is symmetric. Although the adiabatic frame is physically more intuitive and relies on weaker assumptions regarding the electronic states, we see that the Schrödinger Equation for the nuclear wave function is significantly simpler in the diabatic frame (Equation (7)) than in the adiabatic frame (Equation (3)). In particular, the coupling terms in Equation (4) act as derivative operators, while the coupling terms in Equation (8) are multiplicative.

The simplest setting to study electronic state transitions is a two-state PE landscape. In this setting, we assume the existence of exactly two distinct electronic eigenstates ϕ_1 and ϕ_2 . We call ϕ_1 the electronic ground state and ϕ_2 the electronic excited state. The associated nuclear functions are the ground state (nuclear) function χ_1 and the excited state (nuclear) function χ_2 . The diabatic PE landscape has two PE surfaces, V_{11}^D and V_{22}^D , and there is a single coupling term V_{12}^D . Thanks to the coupling term, the evolution of one nuclear wave function has an immediate influence on the evolution of the other. Consider, for example, the initial condition $\chi_1(\mathbf{X}) = 0$. Equation (6) then implies $\langle \chi_2 | \chi_2 \rangle = 1$. That is, the molecule is initially excited. But with time, it is possible that the evolution of χ_2 can cause χ_1 to attain nonzero

values by virtue of the coupling term. This process is electronic de-excitation, or state transition; since $\langle \chi_1 | \chi_1 \rangle$ is the probability of observing the molecule in the electronic ground state, its increase implies de-excitation. We refer to the quantity,

$$\mathbf{G} = \langle \chi_1 | \chi_1 \rangle, \quad (9)$$

as the ground state population. An interesting result relating to electronic de-excitation is the following: A nuclear configuration \mathbf{X} satisfying the system

$$\begin{cases} V_{11}^D(\mathbf{X}) = V_{22}^D(\mathbf{X}) \\ V_{12}^D(\mathbf{X}) = 0 \end{cases}$$

also satisfies $V_1^A(\mathbf{X}) = V_2^A(\mathbf{X})$, or equivalently $E_1(\mathbf{X}) = E_2(\mathbf{X})$. Such a nuclear configuration is called a point of coincidence. In other words, a nuclear configuration at which the diabatic PE surfaces intersect is a point of electronic degeneracy. Such points of coincidence or electronic degeneracy are important in molecular dynamics, as they act as “funnels” through which the excited state function χ_2 can smoothly transition from the upper PE surface to the lower PE surface. This process of electronic de-excitation is more efficient and complete, since now both χ_1 and χ_2 correspond to the electronic ground state ϕ_1 [1].

For our study, we are interested in modeling the time evolution of a nuclear wave function in the diabatic frame. We describe a numerical scheme for implementing Equation (7) computationally. There exists a simple recursive method to model the incidence of a one-dimensional wave function on a potential barrier [2], and we extend this method to the more complicated situation of a molecule with two nuclear degrees of freedom evolving in a PE landscape with two PE surfaces. Our method involves

the discretization of functions into finite vectors and linear operators into square matrices. Instead of using matrix inversion, we produce a recursive method that takes maximum advantage of the sparseness of the square matrices. While large-scale computational models have been constructed to simulate real molecular complexes, our study differs from this in one important way: The aim of our study is not to provide a realistic simulation of complicated molecular dynamics. Rather, our aim is to understand the most basic physical implications of Equation (7). In particular, our aim is to understand how the probability of an electronic de-excitation depends on the internal shape (or nuclear configuration) of the molecule and more generally on the structure of the PE landscape. To reach this end, we construct a model with enough complexity for studying the motion of nuclei and electronic state transitions, but also with enough simplicity that causal relationships are not blurred by additional third-party factors. Concretely, we study how the evolution of a nuclear wave function (provided an initial condition) varies with a set of parameters specifying the shapes of the PE surfaces comprising the PE landscape. The “evolution” is recorded in the form of expectation values of various observables computed at regular time increments. Our study consists of three main phases: the one-dimensional single-state case, the one-dimensional two-state case, and the two-dimensional two-state case.

1.2 The One-Dimensional Single-State Case

In Phase 1, we model the internal nuclear motion of a diatomic molecule. We assume that the PE landscape for the molecule comprises a single PE surface; we assume that there is a unique electronic eigenstate ϕ such that the molecular wave func-

tion is $\Psi(\mathbf{x}, \mathbf{X}, t) = \chi(\mathbf{X}, t)\phi(\mathbf{x})$, where χ is the nuclear wave function. Under this assumption, the PE matrix in Equation (8) reduces to a scalar function V .

Let M_1 and M_2 be the masses of the nuclei, and \mathbf{X}_1 and \mathbf{X}_2 be their positions. Since we are only interested in the internal motion of the molecule, we keep track only of the distance between the two nuclei and not their absolute positions (hence, the system is one-dimensional). Define the coordinate

$$X = \frac{\sqrt{2\mu}}{\hbar} (|\mathbf{X}_1 - \mathbf{X}_2| - X_0), \quad (10)$$

where $\mu = \frac{M_1 M_2}{M_1 + M_2}$ is the reduced mass and X_0 is the equilibrium inter-nuclear distance. Then, $X = 0$ is the equilibrium configuration, $X < 0$ is a compressed configuration, and $X > 0$ is a stretched configuration. Further, under Equation (10), the KE operator transforms as

$$\sum_i -\frac{\hbar^2}{2M_i} \frac{\partial^2}{\partial X_i^2} \rightarrow -\frac{\partial^2}{\partial X^2}.$$

Letting $\hat{\mathbf{T}}$ and $\hat{\mathbf{V}}$ be the KE and PE operators respectively, the nuclear Hamiltonian is given by

$$\hat{\mathbf{H}} = \hat{\mathbf{T}} + \hat{\mathbf{V}} = -\frac{\partial^2}{\partial X^2} + V(X). \quad (11)$$

The evolution of the nuclear wave function is then given by the Schrödinger Equation:

$$\frac{\partial}{\partial t} \chi(X, t) = -i\hat{\mathbf{H}}\chi(X, t). \quad (12)$$

We are primarily interested in the general shape of the nuclear wave function and its evolution with time. For this reason, we let $\hbar = 1$ in Equation (12) for convenience.

For the initial wave function at time $t = 0$, we use a Gaussian wave packet of the form

$$\chi(X, 0) = e^{-AX^2}, \quad (13)$$

where A is a model parameter for which various values are tested. The wave function is normalized before it is used.

We do not compute the electronic eigenstates for the molecule, and so we do not use Equation (8) to derive an expression for the PE function V . Instead, we simply assume a form for the PE function that we think is reasonable and that we are interested in modeling. We select the Morse potential, which models the vibration and dissociation of a diatomic molecule (Figure 1). We use a Morse potential of the form

$$V(X) = 10(1 - e^{-0.1X})^2. \quad (14)$$

Since X effectively tracks the vibration of the molecule, we refer to X as the “vibronic coordinate”.

As the wave function evolves, we collect data at regular time intervals in the form of expectation values of various physical observables, including: the vibronic coordinate, momentum, kinetic energy, potential energy, and total energy.

1.3 The One-Dimensional Two-State Case

In Phase 2, we consider the same diatomic molecule from Phase 1, and we use the same coordinate X (given by Equation (10)) to track the motion of the molecule. But we now extend the PE landscape to comprise two PE surfaces. Let $V_1(X)$ and $V_2(X)$ be the lower and upper PE surfaces respectively, and let $V_{12}(X)$ be the coupling potential. We are then assuming the existence of two orthonormal electronic eigenstates ϕ_1 and ϕ_2 such that the molecular wave function is given by

$$\Psi(X, t) = \chi_1(X, t)\phi_1(X) + \chi_2(X, t)\phi_2(X),$$

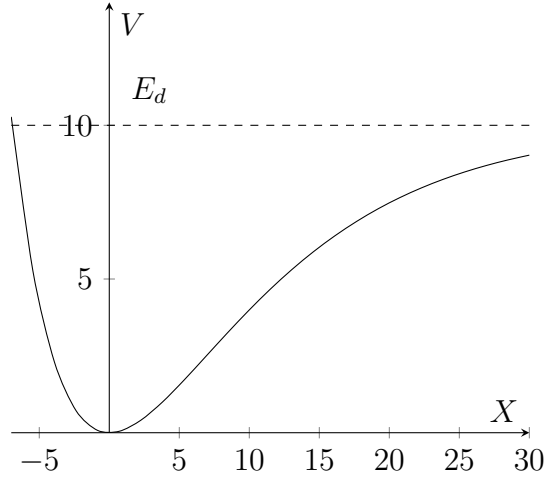


Figure 1: Plot of the Morse PE function $V(X)$. The horizontal asymptote of $V(X)$ is the dissociation energy E_d .

where χ_1 and χ_2 are the ground and excited (nuclear) state functions respectively.

That is, the nuclear wave function χ generalizes to the vector

$$\chi(X, t) = \begin{bmatrix} \chi_1(X, t) \\ \chi_2(X, t) \end{bmatrix}. \quad (15)$$

Similarly, the Hamiltonian generalizes to the matrix

$$\hat{\mathbf{H}} = \begin{bmatrix} \hat{\mathbf{H}}_1 & \hat{\mathbf{H}}_{12} \\ \hat{\mathbf{H}}_{21} & \hat{\mathbf{H}}_2 \end{bmatrix} = \begin{bmatrix} 1 & 0 \\ 0 & 1 \end{bmatrix} \hat{\mathbf{T}} + \begin{bmatrix} \hat{\mathbf{V}}_1 & \hat{\mathbf{V}}_{12} \\ \hat{\mathbf{V}}_{12} & \hat{\mathbf{V}}_2 \end{bmatrix} \quad (16)$$

$$= \begin{bmatrix} \hat{\mathbf{T}} + V_1(X) & V_{12}(X) \\ V_{12}(X) & \hat{\mathbf{T}} + V_2(X) \end{bmatrix}, \quad (17)$$

where $\hat{\mathbf{T}} = -\frac{\partial^2}{\partial X^2}$. This is in accordance with Equation (7). The evolution of the wave function χ is still given by Equation (12).

For the initial wave function, we use a purely excited Gaussian wave packet of the form

$$\chi(X, t) = \begin{bmatrix} \chi_1(X, 0) \\ \chi_2(X, 0) \end{bmatrix} = \begin{bmatrix} 0 \\ \exp^{-5X^2} \end{bmatrix}. \quad (18)$$

The wave function is normalized in accordance with Equation (6) before it is used.

As in Phase 1, we do not compute expressions for the studied PE functions. Instead, we choose expressions for the PE functions that we are interested in studying. We let the ground state PE function be the Morse potential that encourages equilibrium. Let the excited state PE function have a form that encourages molecular expansion and dissociation. Let the coupling potential be a Gaussian that is strongest at the equilibrium configuration (Figure 2). The PE functions are chosen to have the forms

$$V_1(X) = A(1 - e^{-0.1X})^2 \quad (19)$$

$$V_2(X) = B - \frac{10}{1 + e^{-0.1X}} \quad (20)$$

$$V_{12}(X) = Ce^{-D(X-E)^2}, \quad (21)$$

where A, B, C, D, E are positive model parameters. Note that since $V_{12}(X) > 0$ for all X , there is no point of electronic degeneracy.

We monitor the expectation values of the same observables listed for Phase 1. We additionally monitor two more observables: the force defined in terms of a potential gradient, and the ground state population given by Equation (9).

1.4 The Two-Dimensional Two-State Case

In Phase 3, we consider a molecule with two nuclear degrees of freedom. In particular, we consider a molecule that can be constructed by attaching “appendages” to the ends of a diatomic molecule. In this way, the original diatomic molecule acts as an axis around which the appendages can rotate. This introduces a second dimension in

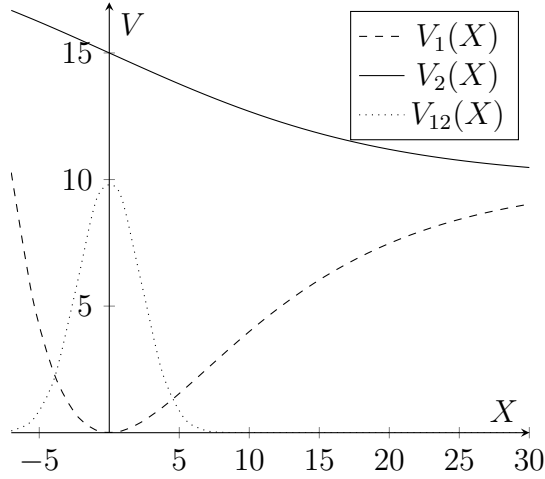


Figure 2: Plots of the Morse potential $V_1(X)$, the repelling potential $V_2(X)$, and the coupling potential $V_{12}(X)$ for the case $(A, B, C, D, E) = (10, 20, 10, 0.1, 0)$.

which the molecule can twist. A unique configuration of the molecule is specified by the vibronic coordinate X , which relates to the length of the diatomic axis, and the torsion angle θ about the axis, $-\pi \leq \theta \leq \pi$.

Let $V_1(X, \theta)$ and $V_2(X, \theta)$ be the two PE surfaces comprising the two-state PE landscape, and let $V_{12}(X, \theta)$ be the coupling PE function. In this two-state system, the nuclear wave function is the vector

$$\chi(X, \theta, t) = \begin{bmatrix} \chi_1(X, \theta, t) \\ \chi_2(X, \theta, t) \end{bmatrix}, \quad (22)$$

and the Hamiltonian takes the form

$$\hat{\mathbf{H}} = \begin{bmatrix} \hat{\mathbf{H}}_1 & \hat{\mathbf{H}}_{12} \\ \hat{\mathbf{H}}_{21} & \hat{\mathbf{H}}_2 \end{bmatrix} = \begin{bmatrix} 1 & 0 \\ 0 & 1 \end{bmatrix} (\hat{\mathbf{T}}_X + \hat{\mathbf{T}}_\theta) + \begin{bmatrix} \hat{\mathbf{V}}_1 & \hat{\mathbf{V}}_{12} \\ \hat{\mathbf{V}}_{12} & \hat{\mathbf{V}}_2 \end{bmatrix} \quad (23)$$

$$= \begin{bmatrix} \hat{\mathbf{T}}_X + \hat{\mathbf{T}}_\theta + V_1(X, \theta) & V_{12}(X, \theta) \\ V_{12}(X, \theta) & \hat{\mathbf{T}}_X + \hat{\mathbf{T}}_\theta + V_2(X, \theta) \end{bmatrix}, \quad (24)$$

where $\hat{\mathbf{T}}_X$ and $\hat{\mathbf{T}}_\theta$ are the KE operators with respect to X and θ . Since we are again interested only in the shape of the nuclear wave function as it evolves, we assume that

the molecule has a moment of inertia about its axis corresponding to the variable X such that the total KE operator takes the form

$$\hat{\mathbf{T}} = \hat{\mathbf{T}}_X + \hat{\mathbf{T}}_\theta = -\frac{\partial^2}{\partial X^2} - \frac{\partial^2}{\partial \theta^2}. \quad (25)$$

The evolution of the wave function is then given by The Schrödinger Equation in two dimensions:

$$\frac{\partial}{\partial t}\chi(X, \theta, t) = -i\hat{\mathbf{H}}\chi(X, \theta, t). \quad (26)$$

For the initial wave function, we use a purely excited Gaussian wave packet. For the wave function to be periodic with respect to the torsion angle θ , we require the boundary condition

$$\chi(X, -\pi, t) = \chi(X, \pi, t), \text{ for all } X, t \quad (27)$$

We let the initial wave function have the form

$$\chi(X, \theta, 0) = \begin{bmatrix} \chi_1(X, \theta, 0) \\ \chi_2(X, \theta, 0) \end{bmatrix} = \begin{bmatrix} 0 \\ e^{-5(X-X_0)^2 - 5(|\theta-\theta_0+\pi|-\pi)^2} \end{bmatrix}, \quad (28)$$

where X_0 and θ_0 are model parameters, with the restriction $0 \leq \theta_0 \leq \pi$. The initial wave function is defined so that it attains its maximum value with respect to θ at $\theta = \theta_0$ and its minimum value at $\theta = \theta_0 - \pi$. The initial wave function is normalized before it is used.

We choose expressions for the PE functions that model the example of cis-trans isomerization. Let $\theta = 0$ correspond to the cis configuration of the molecule. Then, $\theta = \pm\pi$ corresponds to the trans configuration. We define the ground state PE function V_1 such that in the ground state, the cis configuration ($\theta = 0$) is stable and the trans configuration ($\theta = \pm\pi$) is unstable. In contrast, we define the excited state

PE function V_2 such that in the excited state, the cis configuration is unstable and the trans configuration is stable. Thus, V_1 encourages the molecule to twist into the cis configuration, and V_2 encourages the molecule to twist into the trans configuration (Figure 3a). Additionally, both V_1 and V_2 are defined so that the vibration of the molecule along the axis of torsion is harmonic. We let the coupling potential V_{12} be independent of the torsion angle and depend linearly on X (Figure 3b). Thus, we let the PE functions have the forms

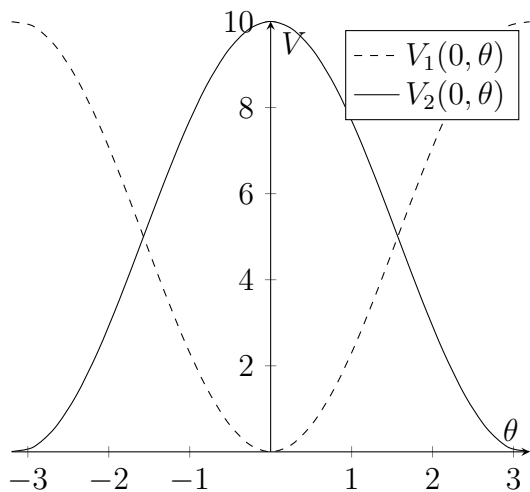
$$V_1(X, \theta) = 0.1X^2 + 5(1 - \cos \theta). \quad (29)$$

$$V_2(X, \theta) = 0.1X^2 + 10 - 5(1 - \cos \theta). \quad (30)$$

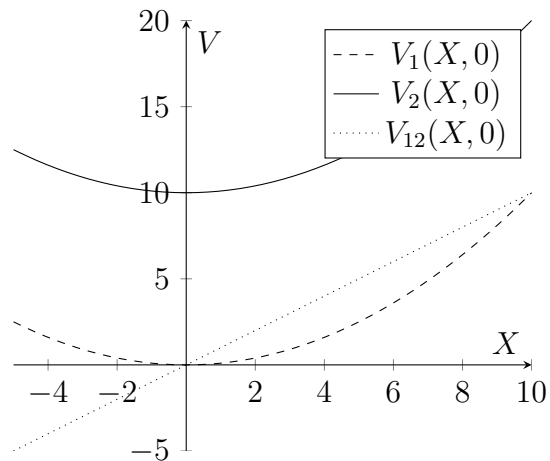
$$V_{12}(X, \theta) = X. \quad (31)$$

Note that the surfaces V_1 and V_2 are completely symmetric with respect to one another. In particular, $V_1(X, \theta + \pi) = V_2(X, \theta)$ for all X, θ . Note also that $V_1(0, \frac{\pi}{2}) = V_2(0, \frac{\pi}{2})$ and $V_{12}(0, \frac{\pi}{2}) = 0$. Thus, the molecular configuration $(X, \theta) = (0, \frac{\pi}{2})$ is a point of electronic degeneracy [1].

The physical observables for which we monitor expectation values include: the vibronic coordinate, absolute torsion angle, kinetic energy, potential energy, total energy, vibronic force (along the axis of torsion), torque (force with respect to the absolute torsion angle), and ground state population.



(a) Plots of the ground state potential $V_1(0, \theta)$ and excited state potential $V_2(0, \theta)$ as functions of θ . These are angular profiles of V_1 and V_2 for $X = 0$. The coupling potential is not shown, since $V_{12}(0, \theta) = 0$.



(b) Plots of the ground state potential $V_1(X, 0)$, excited state potential $V_2(X, 0)$, and coupling potential $V_{12}(X, 0)$ as functions of X . These are profiles of V_1 , V_2 , and V_{12} for $\theta = 0$.

Figure 3: Plots of some sectional curves of the PE functions.

2 Methodology

Our numerical model for the time evolution of a nuclear wave function is based on the recursive method proposed by Lösch [2]. This involves the discretization of functions into finite vectors and linear operators into square matrices. Further, it involves the application of the Crank-Nicolson method to the time-dependent Schrödinger Equation in order to derive its Cayley form. This leads to a tridiagonal system of difference equations that can be easily solved numerically. We implement our model in the programming language FORTRAN.

2.1 The One-Dimensional Single-State Case

Consider a diatomic molecule whose nuclear configuration is specified by the coordinate X given in Equation (10). Define $\chi(X, t)$ to be the nuclear wave function at time t . Let $V(X)$ be the effective nuclear PE curve in which the wave function evolves. Recall that the Hamiltonian is given by Equation (11) and that the evolution of χ is given by Equation (12).

The construction of our numerical model begins with the discretization of space and time. Let ΔX and Δt be the sizes of the space step and time step respectively. We approximate the infinite space interval by a suitably large but finite interval $[X_1, X_2]$, $X_1 < 0 < X_2$. We denote the discretized wave function and PE function at the j th space step and n th time step by χ_j^n and V_j :

$$\chi_j^n = \chi(X_1 + j\Delta X, n\Delta t). \quad (32)$$

$$V_j = V(X_1 + j\Delta X). \quad (33)$$

At a fixed time n , χ^n and \mathbf{V} are vectors with components χ_j^n and V_j respectively. Using the central difference approximation for the second derivative, the action of the discretized Hamiltonian on the discretized wave function yields a vector $\hat{\mathbf{H}}\chi^n$ with components

$$\begin{aligned} [\hat{\mathbf{H}}\chi^n]_j &= - \left(\frac{\chi_{j+1}^n - 2\chi_j^n + \chi_{j-1}^n}{(\Delta X)^2} \right) + \mathbf{V}_j \chi_j^n \\ &= \frac{-\chi_{j-1}^n + (2 + (\Delta X)^2 \mathbf{V}_j) \chi_j^n - \chi_{j+1}^n}{(\Delta X)^2}. \end{aligned} \quad (34)$$

The discretized time-dependent Schrödinger Equation takes the form

$$\frac{\Delta \chi^n}{\Delta t} = -i \hat{\mathbf{H}} \chi^n,$$

yielding the difference equation

$$\Delta \chi^n = -i \Delta t \hat{\mathbf{H}} \chi^n. \quad (35)$$

Applying Equation (35) to χ^n and χ^{n+1} , each for a time $\frac{\Delta t}{2}$, yields the equations

$$\Delta \chi^n = -\frac{i \Delta t}{2} \hat{\mathbf{H}} \chi^n. \quad (36)$$

$$\Delta \chi^{n+1} = -\frac{i \Delta t}{2} \hat{\mathbf{H}} \chi^{n+1}. \quad (37)$$

Let $\alpha = \frac{i \Delta t}{2}$ for brevity. Using a forward difference for Equation (36) and a backward difference for Equation (37), we get

$$\chi^{n+\frac{1}{2}} - \chi^n = -\alpha \hat{\mathbf{H}} \chi^n.$$

$$\chi^{n+1} - \chi^{n+\frac{1}{2}} = -\alpha \hat{\mathbf{H}} \chi^{n+1}.$$

Adding these two equations and regrouping terms, we arrive at the Cayley approximation for the Schrödinger Equation:

$$(1 + \alpha \hat{\mathbf{H}}) \chi^{n+1} = (1 - \alpha \hat{\mathbf{H}}) \chi^n. \quad (38)$$

Note that the exact solution to Equation (12) is $\chi(X, t) = \exp(-i\hat{\mathbf{H}}t)\chi(X, 0)$, where the operator $\exp(-i\hat{\mathbf{H}}t)$ is defined in terms of its Taylor expansion. The Cayley operator

$$\hat{\mathbf{C}} = (1 + \alpha\hat{\mathbf{H}})^{-1}(1 - \alpha\hat{\mathbf{H}})$$

is a good approximation to $\exp(-i\Delta t\hat{\mathbf{H}})$. Note also that $\hat{\mathbf{C}}$ is unitary, so that Equation (38) preserves the norm of the wave function.

We simplify Equation (38) further by performing a variable substitution [2]. Define the vector

$$\zeta = \chi^n + \chi^{n+1}. \quad (39)$$

Performing the substitution $\chi^{n+1} = \zeta - \chi^n$ in Equation (38) yields

$$(1 + \alpha\hat{\mathbf{H}})(\zeta - \chi^n) = (1 - \alpha\hat{\mathbf{H}})\chi^n.$$

Distributing the operator on the left side,

$$(1 + \alpha\hat{\mathbf{H}})\zeta - (1 + \alpha\hat{\mathbf{H}})\chi^n = (1 - \alpha\hat{\mathbf{H}})\chi^n.$$

Moving the second term on the left side to the right, we obtain

$$\begin{aligned} (1 + \alpha\hat{\mathbf{H}})\zeta &= (1 - \alpha\hat{\mathbf{H}})\chi^n + (1 + \alpha\hat{\mathbf{H}})\chi^n \\ &= (1 - \alpha\hat{\mathbf{H}} + 1 + \alpha\hat{\mathbf{H}})\chi^n \\ &= 2\chi^n. \end{aligned}$$

As χ^n is known, our goal is to solve for ζ . Once this is done, we obtain χ^{n+1} using Equation (39). We therefore arrive at a set of difference equations that allow us to

find χ^{n+1} given χ^n :

$$(1 + \alpha \hat{\mathbf{H}})\zeta = 2\chi^n. \quad (40)$$

$$\chi^{n+1} = \zeta - \chi^n. \quad (41)$$

This set of equations is not to be solved simultaneously but instead as a loop running over n . The wave function evolves in time via this recursive loop. Note that ζ is redefined when solved from Equation (40) in every recurrence.

Using Equation (34), the above equations can be stated more explicitly as

$$-\beta\zeta_{j-1} + [1 + \beta(2 + (\Delta X)^2 V_j)]\zeta_j - \beta\zeta_{j+1} = 2\chi_j^n \quad (42)$$

$$\chi_j^{n+1} = \zeta_j - \chi_j^n, \quad (43)$$

where $\beta = \frac{\alpha}{(\Delta X)^2}$, and where one equation is looped over all j before proceeding to the next equation or the next value of n . Notice that Equation (42) is a tridiagonal linear system (indexed by j). This system can be easily and efficiently solved using the Tridiagonal Algorithm— a simple Gaussian elimination (or equivalently, an LU factorization) that takes advantage of the sparsity of the system [3].

2.2 The One-Dimensional Two-State Case

We proceed to extend the above method to the more general case of a PE landscape with two PE surfaces given by V_1 and V_2 and a coupling potential given by V_{12} .

Recall that the wave function $\chi(X, t)$ and the Hamiltonian $\hat{\mathbf{H}}$ generalize to a vector and matrix given by Equations (15) and (17) respectively. With these generalizations,

Equation (38) takes the form

$$\left(\begin{bmatrix} 1 & 0 \\ 0 & 1 \end{bmatrix} + \alpha \begin{bmatrix} \hat{\mathbf{H}}_1 & \hat{\mathbf{H}}_{12} \\ \hat{\mathbf{H}}_{21} & \hat{\mathbf{H}}_2 \end{bmatrix} \right) \begin{bmatrix} \chi_1^{n+1} \\ \chi_2^{n+1} \end{bmatrix} = \left(\begin{bmatrix} 1 & 0 \\ 0 & 1 \end{bmatrix} - \alpha \begin{bmatrix} \hat{\mathbf{H}}_1 & \hat{\mathbf{H}}_{12} \\ \hat{\mathbf{H}}_{21} & \hat{\mathbf{H}}_2 \end{bmatrix} \right) \begin{bmatrix} \chi_1^n \\ \chi_2^n \end{bmatrix},$$

where χ_1^n and χ_2^n are the discretized ground state and excited state wave functions.

This matrix equation is equivalent to the linear system

$$(1 + \alpha \hat{\mathbf{H}}_1) \chi_1^{n+1} + \alpha \hat{\mathbf{V}}_{12} \chi_2^{n+1} = (1 - \alpha \hat{\mathbf{H}}_1) \chi_1^n - \alpha \hat{\mathbf{V}}_{12} \chi_2^n. \quad (44)$$

$$\alpha \hat{\mathbf{V}}_{12} \chi_1^{n+1} + (1 + \alpha \hat{\mathbf{H}}_2) \chi_2^{n+1} = -\alpha \hat{\mathbf{V}}_{12} \chi_1^n + (1 - \alpha \hat{\mathbf{H}}_2) \chi_2^n, \quad (45)$$

where we used the fact that $\hat{\mathbf{H}}_{12} = \hat{\mathbf{H}}_{21} = \hat{\mathbf{V}}_{12}$.

Due to the coupling term appended to each equation, Equations (44) and (45) are no longer tridiagonal systems. To handle this increase in complexity, we propose a scheme that is analogous to the application of the Alternating Direction Implicit (ADI) Method to two-dimensional diffusion equations [3]. Essentially, our strategy is to forward the wave function one state at a time; while forwarding one state, we hold the other fixed. Our scheme exploits the fact that for small enough Δt , $\chi_1^n \approx \chi_1^{n+1}$ and $\chi_2^n \approx \chi_2^{n+1}$. First, while forwarding the ground state function χ_1^n to χ_1^{n+1} , we assume that χ_2^n is constant for one forward time step. Second, while forwarding the excited state function χ_2^n to χ_2^{n+1} , we assume that χ_1^{n+1} is constant for one backward time step. To implement this scheme, we approximate χ_2^{n+1} by χ_2^n in Equation (44), and we approximate χ_1^n by χ_1^{n+1} in Equation (45). These approximations yield

$$(1 + \alpha \hat{\mathbf{H}}_1) \chi_1^{n+1} + \alpha \hat{\mathbf{V}}_{12} \chi_2^n = (1 - \alpha \hat{\mathbf{H}}_1) \chi_1^n - \alpha \hat{\mathbf{V}}_{12} \chi_2^n.$$

$$\alpha \hat{\mathbf{V}}_{12} \chi_1^{n+1} + (1 + \alpha \hat{\mathbf{H}}_2) \chi_2^{n+1} = -\alpha \hat{\mathbf{V}}_{12} \chi_1^n + (1 - \alpha \hat{\mathbf{H}}_2) \chi_2^{n+1}.$$

Moving the coupling terms to the right side, we get

$$(1 + \alpha \hat{\mathbf{H}}_1) \chi_1^{n+1} = (1 - \alpha \hat{\mathbf{H}}_1) \chi_1^n - 2\alpha \hat{\mathbf{V}}_{12} \chi_2^n. \quad (46)$$

$$(1 + \alpha \hat{\mathbf{H}}_2) \chi_2^{n+1} = -\alpha \hat{\mathbf{V}}_{12} \chi_1^n + (1 - 2\alpha \hat{\mathbf{H}}_2) \chi_2^{n+1}. \quad (47)$$

Just as we did to simplify Equation (38) to Equation (40), we perform the substitutions

$$\zeta_i = \chi_i^n + \chi_i^{n+1}, \quad i = 1, 2$$

to simplify Equations (46) and (47) to arrive at a simpler set of difference equations through which we can loop in order to find χ^{n+1} given χ^n :

$$\frac{1}{2}(1 + \alpha \hat{\mathbf{H}}_1) \zeta_1 = \chi_1^n - \alpha \hat{\mathbf{V}}_{12} \chi_2^n. \quad (48)$$

$$\chi_1^{n+1} = \zeta_1 - \chi_1^n. \quad (49)$$

$$\frac{1}{2}(1 + \alpha \hat{\mathbf{H}}_2) \zeta_2 = \chi_2^n - \alpha \hat{\mathbf{V}}_{12} \chi_1^{n+1}. \quad (50)$$

$$\chi_2^{n+1} = \zeta_2 - \chi_2^n. \quad (51)$$

Like Equations (40) and (41), these four equations are solved in the fashion of a loop running over n . Note that when we get to Equation (50) in the loop, χ_1^{n+1} is known thanks to the preceding equations. Thus, the right sides of Equations (48) and (50) are known vector quantities, and their left sides are equivalent to the left side of Equation (40). Therefore, Equations (48) and (50) are tridiagonal systems that can be easily solved using the Tridiagonal Algorithm.

2.3 The Two-Dimensional Two-State Case

We proceed to generalize the above method to the case of a PE landscape that consists of two-dimensional surfaces. The functions χ , V_1 , V_2 , and V_{12} now depend on two nuclear degrees of freedom—the vibronic coordinate X and the torsion angle θ .

We discretize the intervals for X and t in the same way as in the one-dimensional case. We discretize the interval $[-\pi, \pi]$ for the new coordinate θ such that the angular step size is also ΔX . Then, the values of the wave function and PE functions at the (i, j) th space step (i.e., at the i th step in X and j th step in θ) and n th time step are denoted and given by

$$[\chi_1]_{i,j}^n = \chi_1(X_1 + i\Delta X, -\pi + j\Delta X, n\Delta t). \quad (52)$$

$$[\chi_2]_{i,j}^n = \chi_2(X_1 + i\Delta X, -\pi + j\Delta X, n\Delta t). \quad (53)$$

$$[V_1]_{i,j} = V_1(X_1 + i\Delta X, -\pi + j\Delta X). \quad (54)$$

$$[V_2]_{i,j} = V_2(X_1 + i\Delta X, -\pi + j\Delta X). \quad (55)$$

$$[V_{12}]_{i,j} = V_{12}(X_1 + i\Delta X, -\pi + j\Delta X). \quad (56)$$

For a fixed time step n , we define χ_1^n , χ_2^n , \mathbf{V}_1 , \mathbf{V}_2 , and \mathbf{V}_{12} to be the matrices with entries indexed by i, j and are listed above. The actions of the partial KE operators $\hat{\mathbf{T}}_X$ and $\hat{\mathbf{T}}_\theta$ on a discretized wave function χ^n return matrices $\hat{\mathbf{T}}_X \chi^n$ and $\hat{\mathbf{T}}_\theta \chi^n$ with

entries given by

$$[\hat{\mathbf{T}}_X \chi^n]_{i,j} = \frac{-\chi_{i-1,j}^n + 2\chi_{i,j}^n - \chi_{i+1,j}^n}{(\Delta X)^2}. \quad (57)$$

$$[\hat{\mathbf{T}}_\theta \chi^n]_{i,j} = \frac{-\chi_{i,j-1}^n + 2\chi_{i,j}^n - \chi_{i,j+1}^n}{(\Delta X)^2}. \quad (58)$$

$$(59)$$

The discretized Hamiltonian $\hat{\mathbf{H}}$ is then obtained by combining the discretized KE and PE operators together in accordance with Equation (24).

Since we are still considering a two-state PE landscape, Equations (46) and (47) are valid even in two dimensions. But due to the more complicated KE operator $\hat{\mathbf{T}} = \hat{\mathbf{T}}_X + \hat{\mathbf{T}}_\theta$, Equations (46) and (47) are not tridiagonal systems in two dimensions. Therefore, further simplification of Equations (46) and (47) is required. We use the ADI method for two-dimensional diffusion problems [3]. In Equation (46), we forward χ_1^n to χ_1^{n+1} while holding χ_2^n fixed. In the ADI method, we forward χ_1^n to χ_1^{n+1} in two half-steps, with $\chi_1^{n+\frac{1}{2}}$ as the intermediate wave function. Thus, Equation (46) transforms into a set of two equations:

$$\left[1 + \frac{1}{2}\alpha(\hat{\mathbf{T}}_X + \hat{\mathbf{T}}_\theta + \hat{\mathbf{V}}_1)\right] \chi_1^{n+\frac{1}{2}} = \left[1 - \frac{1}{2}\alpha(\hat{\mathbf{T}}_X + \hat{\mathbf{T}}_\theta + \hat{\mathbf{V}}_1)\right] \chi_1^n - 2\left(\frac{1}{2}\alpha\right) \hat{\mathbf{V}}_{12}\chi_2^n \quad (60)$$

$$\left[1 + \frac{1}{2}\alpha(\hat{\mathbf{T}}_X + \hat{\mathbf{T}}_\theta + \hat{\mathbf{V}}_1)\right] \chi_1^{n+1} = \left[1 - \frac{1}{2}\alpha(\hat{\mathbf{T}}_X + \hat{\mathbf{T}}_\theta + \hat{\mathbf{V}}_1)\right] \chi_1^{n+\frac{1}{2}} - 2\left(\frac{1}{2}\alpha\right) \hat{\mathbf{V}}_{12}\chi_2^n, \quad (61)$$

where the Hamiltonian $\hat{\mathbf{H}}_1$ is made explicit, and $\alpha = \frac{i\Delta t}{2}$ is replaced with $\frac{1}{2}\alpha$ due to the half-step. For Equation (60), we can approximate $\hat{\mathbf{T}}_X \chi_1^n$ by $\hat{\mathbf{T}}_X \chi_1^{n+\frac{1}{2}}$ and $\hat{\mathbf{T}}_\theta \chi_1^{n+\frac{1}{2}}$ by $\hat{\mathbf{T}}_\theta \chi_1^n$. These approximations are valid for a small enough time step size Δt . For

Equation (61), we can approximate $\hat{\mathbf{T}}_\theta \chi_1^{n+\frac{1}{2}}$ by $\hat{\mathbf{T}}_\theta \chi_1^{n+1}$ and $\hat{\mathbf{T}}_X \chi_1^{n+1}$ by $\hat{\mathbf{T}}_X \chi_1^{n+\frac{1}{2}}$. Notice that the approximations we want to make in the second half-step (i.e., to Equation (61)) are complementary to the approximations in the first half-step (i.e., to Equation (60)). This is to maintain the intrinsic symmetry between $\hat{\mathbf{T}}_X$ and $\hat{\mathbf{T}}_\theta$ in the limit $\Delta t \rightarrow 0$. Making all of these approximations and gathering terms of like time steps, Equations (60) and (61) transform to

$$\begin{aligned} \left[1 + \frac{1}{2}\alpha(\hat{\mathbf{T}}_X + \hat{\mathbf{T}}_X + \hat{\mathbf{V}}_1)\right] \chi_1^{n+\frac{1}{2}} &= \left[1 - \frac{1}{2}\alpha(\hat{\mathbf{T}}_\theta + \hat{\mathbf{T}}_\theta + \hat{\mathbf{V}}_1)\right] \chi_1^n - \alpha \hat{\mathbf{V}}_{12} \chi_2^n. \\ \left[1 + \frac{1}{2}\alpha(\hat{\mathbf{T}}_\theta + \hat{\mathbf{T}}_\theta + \hat{\mathbf{V}}_1)\right] \chi_1^{n+1} &= \left[1 - \frac{1}{2}\alpha(\hat{\mathbf{T}}_X + \hat{\mathbf{T}}_X + \hat{\mathbf{V}}_1)\right] \chi_1^{n+\frac{1}{2}} - \alpha \hat{\mathbf{V}}_{12} \chi_2^n. \end{aligned}$$

We can apply the ADI method to Equation (47) in the same way as we did for Equation (46). In this way, we obtain a set of difference equations from which we can solve for χ^{n+1} given χ^n :

$$\left[1 + \alpha \left(\hat{\mathbf{T}}_X + \frac{1}{2}\hat{\mathbf{V}}_1\right)\right] \chi_1^{n+\frac{1}{2}} = \left[1 - \alpha \left(\hat{\mathbf{T}}_\theta + \frac{1}{2}\hat{\mathbf{V}}_1\right)\right] \chi_1^n - \alpha \hat{\mathbf{V}}_{12} \chi_2^n. \quad (62)$$

$$\left[1 + \alpha \left(\hat{\mathbf{T}}_\theta + \frac{1}{2}\hat{\mathbf{V}}_1\right)\right] \chi_1^{n+1} = \left[1 - \alpha \left(\hat{\mathbf{T}}_X + \frac{1}{2}\hat{\mathbf{V}}_1\right)\right] \chi_1^{n+\frac{1}{2}} - \alpha \hat{\mathbf{V}}_{12} \chi_2^n. \quad (63)$$

$$\left[1 + \alpha \left(\hat{\mathbf{T}}_X + \frac{1}{2}\hat{\mathbf{V}}_2\right)\right] \chi_2^{n+\frac{1}{2}} = \left[1 - \alpha \left(\hat{\mathbf{T}}_\theta + \frac{1}{2}\hat{\mathbf{V}}_2\right)\right] \chi_2^n - \alpha \hat{\mathbf{V}}_{12} \chi_1^{n+1}. \quad (64)$$

$$\left[1 + \alpha \left(\hat{\mathbf{T}}_\theta + \frac{1}{2}\hat{\mathbf{V}}_2\right)\right] \chi_2^{n+1} = \left[1 - \alpha \left(\hat{\mathbf{T}}_X + \frac{1}{2}\hat{\mathbf{V}}_2\right)\right] \chi_2^{n+\frac{1}{2}} - \alpha \hat{\mathbf{V}}_{12} \chi_1^{n+1}. \quad (65)$$

As usual, this set of equations is solved as a loop running over n . Therefore, the right sides to all four equations are known matrix quantities. Since the operators $\hat{\mathbf{T}}_X$ and $\hat{\mathbf{T}}_\theta$ are on opposite sides in each equation, Equations (62) and (64) are tridiagonal systems that can be easily solved using the Tridiagonal Algorithm. Because of the periodic boundary condition given by Equation (27), Equations (63) and (65), which

have $\hat{\mathbf{T}}_\theta$ operating on their left sides, are not purely tridiagonal systems. Rather, they are cyclic tridiagonal systems. These systems are easily solved by applying the Sherman-Morrison Formula to a simple perturbation of a purely tridiagonal system [3].

2.4 Normalization and Expectation Values

Both the normalization of the initial wave functions and the computation of expectation values utilize the Dirac bracket. We must therefore define the Dirac bracket for discretized arguments. The computation of expectation values additionally requires the discretization of the operators corresponding to the observables we want to monitor. We discretize the bracket and the operators for relevant observables first in one dimension and then in two dimensions.

2.4.1 In One Dimension

Let \mathbf{f}, \mathbf{g} be vectors resulting from the discretization of two arbitrary wave functions $f(X)$ and $g(X)$ respectively. Then, the Dirac bracket of \mathbf{f} and \mathbf{g} is given by the trapezoidal sum

$$\langle \mathbf{f}, \mathbf{g} \rangle = \sum_j \frac{1}{2} (f_j^* g_j + f_{j+1}^* g_{j+1}) \Delta X, \quad (66)$$

where f_j, g_j are the indexed entries of \mathbf{f} and \mathbf{g} respectively.

The discretized initial wave function χ^0 is then normalized by scaling χ^0 so that it satisfies

$$\langle \chi^0 | \chi^0 \rangle = 1. \quad (67)$$

Again, the methods described in the preceding sections ensure a unitary evolution

of the wave function, so that the wave function is approximately normalized for all time.

For both the single-state and two-state cases, we are interested in the following observables: the vibronic coordinate $\hat{\mathbf{X}}$, momentum $\hat{\mathbf{p}}$, kinetic energy $\hat{\mathbf{T}}$, potential energy $\hat{\mathbf{V}}$, and total energy $\hat{\mathbf{H}}$. The action of the vibronic coordinate and momentum operators on the wave function return vectors with the following entries respectively:

$$[\hat{\mathbf{X}}\chi^n]_j = (X_1 + j\Delta X)\chi_j^n. \quad (68)$$

$$[\hat{\mathbf{p}}\chi^n]_j = -\frac{i(\chi_{j+1}^n - \chi_{j-1}^n)}{2\Delta X}. \quad (69)$$

The actions of the KE operator is defined in accordance with Equation (34). If \mathbf{q} is one of $\hat{\mathbf{X}}$, $\hat{\mathbf{p}}$, or $\hat{\mathbf{T}}$, then the expectation value of \mathbf{q} in the single state case at the n th time step is simply

$$\langle \mathbf{q} \rangle = \langle \chi^n | \mathbf{q} | \chi^n \rangle, \quad (70)$$

and the expectation value of \mathbf{q} in the two-state case is

$$\langle \mathbf{q} \rangle = \langle \chi_1^n | \mathbf{q} | \chi_1^n \rangle + \langle \chi_2^n | \mathbf{q} | \chi_2^n \rangle. \quad (71)$$

For any arbitrary discretized PE function \mathbf{V} , the action of the PE operator $\hat{\mathbf{V}}$ on the wave function returns a vector with entries

$$[\hat{\mathbf{V}}\chi^n]_j = V_j\chi_j^n.$$

For the single-state case, the expectation value of $\hat{\mathbf{V}}$ satisfies Equation (70). For the two-state case, the expectation value of $\hat{\mathbf{V}}$ takes a more complicated form due to the coupling potentials:

$$\langle \hat{\mathbf{V}} \rangle = \langle \chi^n | \hat{\mathbf{V}}_1\chi_1^n + \hat{\mathbf{V}}_{12}\chi_2^n \rangle + \langle \chi_2^n | \hat{\mathbf{V}}_{12}\chi_1^n + \hat{\mathbf{V}}_2\chi_2^n \rangle. \quad (72)$$

For both the single-state and two-state cases, the total energy expectation value is given by

$$\langle \hat{\mathbf{H}} \rangle = \langle \hat{\mathbf{T}} \rangle + \langle \hat{\mathbf{V}} \rangle. \quad (73)$$

For the two-state case, we additionally monitor the force $\hat{\mathbf{F}}$. For any arbitrary discretized PE function \mathbf{V} , the action of the corresponding force operator $\hat{\mathbf{F}}$ (which is the negative gradient of \mathbf{V}) on the wave function returns a vector with entries

$$[\hat{\mathbf{F}}\chi^n]_j = -\frac{(\mathbf{V}_{j+1} - \mathbf{V}_{j-1})\chi_j^n}{2\Delta X}. \quad (74)$$

In this way, let $\hat{\mathbf{F}}_1, \hat{\mathbf{F}}_2, \hat{\mathbf{F}}_{12}$ be the force operators corresponding to the PE operators $\hat{\mathbf{V}}_1, \hat{\mathbf{V}}_2$, and $\hat{\mathbf{V}}_{12}$ respectively. Then, the force expectation value is given by

$$\langle \hat{\mathbf{F}} \rangle = \langle \chi^n | \hat{\mathbf{F}}_1\chi_1^n + \hat{\mathbf{F}}_{12}\chi_2^n \rangle + \langle \chi_2^n | \hat{\mathbf{F}}_{12}\chi_1^n + \hat{\mathbf{F}}_2\chi_2^n \rangle. \quad (75)$$

Finally, for the two-state case, we monitor the ground state population, which at the n th time step is given by

$$\mathbf{G} = \langle \chi_1^n | \chi_1^n \rangle. \quad (76)$$

2.4.2 In Two Dimensions

Let \mathbf{f}, \mathbf{g} be matrices resulting from the discretization of two arbitrary wave functions $f(X, \theta)$ and $g(X, \theta)$ respectively. Then, the Dirac bracket of \mathbf{f} and \mathbf{g} is given by the rectangular sum

$$\langle \mathbf{f} | \mathbf{g} \rangle = \sum_{i,j} f_{ij}^* g_{ij} (\Delta X)^2, \quad (77)$$

where f_{ij}, g_{ij} are the indexed entries of \mathbf{f} and \mathbf{g} respectively. The discretized initial wave function χ^0 is normalized by scaling the matrix χ^0 such that it satisfies Equ-

tion (67). By unitarity of our evolution method, the norm of the wave function is conserved.

We are interested in the following observables: the vibronic coordinate $\hat{\mathbf{X}}$, absolute torsion angle $\hat{\theta}$, kinetic energy $\hat{\mathbf{T}}$, potential energy $\hat{\mathbf{V}}$, total energy $\hat{\mathbf{H}}$, vibronic force $\hat{\mathbf{F}}$, torque $\hat{\tau}$, and ground state population \mathbf{G} . The actions of $\hat{\mathbf{X}}$ and $\hat{\theta}$ on the wave function χ^n return matrices that have entries

$$[\hat{\mathbf{X}}\chi^n]_{i,j} = (X_1 + i\Delta X)\chi_{i,j}^n. \quad (78)$$

$$[\hat{\theta}\chi^n]_{i,j} = |-\pi + j\Delta X|\chi_{i,j}^n. \quad (79)$$

We monitor the absolute torsion angle (as given above) instead of the usual signed torsion angle because we are not interested in the direction in which the molecule twists but only in the extent to which the molecule twists away from the cis configuration. In this way, $\hat{\theta} = 0$ and $\hat{\theta} = \pi$ sharply correspond to the cis and trans configurations respectively. The action of the KE operators $\hat{\mathbf{T}}_X$ and $\hat{\mathbf{T}}_\theta$ are defined by Equations (57) and (58). The total KE operator is simply $\hat{\mathbf{T}} = \hat{\mathbf{T}}_X + \hat{\mathbf{T}}_\theta$. The expectation values of $\hat{\mathbf{X}}$, $\hat{\theta}$, and $\hat{\mathbf{T}}$ are given by Equation (71).

For any arbitrary discretized PE function \mathbf{V} , the actions of the PE operator $\hat{\mathbf{V}}$ and the corresponding force and torque operators $\hat{\mathbf{F}}$ and $\hat{\tau}$ on the wave function χ^n return matrices with entries

$$\begin{aligned} [\hat{\mathbf{V}}\chi^n]_{i,j} &= V_{i,j}\chi_{i,j}^n \\ [\hat{\mathbf{F}}\chi^n]_{i,j} &= -\frac{(V_{i+1,j} - V_{i-1,j})\chi_{i,j}^n}{2\Delta X} \\ [\hat{\tau}\chi^n]_{i,j} &= -\frac{\text{sgn}(i)(V_{i,j+1} - V_{i,j-1})\chi_{i,j}^n}{2\Delta X}, \end{aligned} \quad (80)$$

where $\text{sgn}(i) = 1$ if $-\pi + i\Delta X \geq 0$ and $\text{sgn}(i) = -1$ otherwise. The torque is defined to be positive if it forces the molecule to twist away from the cis configuration, and negative otherwise. We define the torque in this way because again we are not concerned with the direction of twisting but only with the extent of twisting away from the cis configuration and towards the trans configuration. The PE and force expectation values are then given by Equations (72) and (75) respectively, and the torque expectation value is given analogously as

$$\langle \hat{\tau} \rangle = \langle \chi_1^n | \hat{\tau}_1 \chi_1^n + \hat{\tau}_{12} \chi_2^n \rangle + \langle \chi_2^n | \hat{\tau}_{12} \chi_1^n + \hat{\tau}_2 \chi_2^n \rangle. \quad (81)$$

The total energy expectation value is given by Equation (73), and the ground state population is given by Equation (76).

3 Results

All figures in this section (Figures 4–13) are presented at the end of the section.

3.1 The One-Dimensional Single-State Case

In Phase 1 of our study, we are interested in the dynamics of a wave packet (Equation (13)) in a Morse potential (Equation (14)). Recall that

$$\chi(X, 0) = e^{-AX^2}$$

$$V(X) = 10(1 - e^{-0.1X})^2,$$

where A is a model parameter, and $E_d = 10$ is the dissociation energy. In our numerical implementation, we use the interval $[X_1, X_2] = [-50, 450]$ with space step size $\Delta X = 0.005$ and time step size $\Delta t = 0.0025$. We model two possible cases: 1) The energy expectation value is less than the dissociation energy ($\langle \hat{\mathbf{H}} \rangle < E_d$), and 2) the energy expectation value is greater than the dissociation energy ($\langle \hat{\mathbf{H}} \rangle > E_d$). We model the two cases by using $A = 4$ and $A = 16$, respectively. For both cases, the energy expectation value is $\langle \hat{\mathbf{H}} \rangle = A$. We observe that total energy is conserved with time, indicating that our model is reasonable (Figures 4c and 4f). In both cases, we observe that $\langle X \rangle$ increases with time; i.e., the diatomic molecule is expanding. Given the 4-fold difference in energy between the two cases (4 vs. 16), we observe a 4-fold difference in $\langle X \rangle$ between the two cases at time $t = 50$ (30 vs. 120) (Figures 4a and 4d). Thus, greater energy directly leads to greater expansion. For both cases, the momentum expectation value is positive and on average decreasing; this is consistent with the molecular expansion that we observe (Figures 4b and 4e). Moreover, the

kinetic energy in Case 2 at $t = 50$ is significantly greater than the kinetic energy in Case 1, increasing the contrast in molecular expansion between the two cases (Figures 4c and 4f). Therefore, the difference in energy between the two cases with respect to the dissociation energy has reasonable consequences. More generally, we conclude that our model for the one-dimensional single-state case is reasonable.

3.2 The One-Dimensional Two-State Case

In Phase 2, we extend the model from phase 1 by introducing a second PE surface as well as a coupling potential. We use the wave packet given by Equation (18) and the PE functions given by Equations (19)–(21):

$$\begin{aligned}\chi_1(X, 0) &= 0 \\ \chi_2(X, 0) &= e^{-5X^2} \\ V_1(X) &= A(1 - e^{-0.1X})^2 \\ V_2(X) &= B - \frac{10}{1 + e^{-0.1X}} \\ V_{12}(X) &= Ce^{-D(X-E)^2},\end{aligned}$$

where A, B, C, D, E are model parameters. We use the interval $[X_1, X_2] = [-50, 250]$ with space step size $\Delta X = 0.002$ and time step size $\Delta t = 0.001$. We test a total of nine cases; the sets of values for the model parameters used for each case are listed in Table 1.

We take Case 1 to be a standard against which we compare the other cases. For each parameter except A , we test a value less than the standard and a value greater than the standard, giving us eight cases in addition to Case 1. We are primarily

| Case | A | B | C | D | E |
|------|-----|-----|-----|------|-----|
| 1 | 10 | 20 | 15 | 0.1 | 0 |
| 2 | 10 | 15 | 15 | 0.1 | 0 |
| 3 | 10 | 25 | 15 | 0.1 | 0 |
| 4 | 10 | 20 | 5 | 0.1 | 0 |
| 5 | 10 | 20 | 25 | 0.1 | 0 |
| 6 | 10 | 20 | 15 | 0.01 | 0 |
| 7 | 10 | 20 | 15 | 1 | 0 |
| 8 | 10 | 20 | 15 | 0.1 | -5 |
| 9 | 10 | 20 | 15 | 0.1 | 5 |

Table 1: List of the model parameter values used for each case of Phase 2.

concerned with the dynamics of the ground state population \mathbf{G} and its dependence on the five model parameters characterizing the relative shapes of the PE functions. We monitor these dynamics over the time interval $[0, 6]$.

In Case 1, the ground state population oscillates with time with a constant frequency and a diminishing amplitude, leading to an asymptotic limit of the ground state population (Figure 5a). Since the coupling potential facilitates state transition in both directions (both de-excitation and excitation), the oscillations are expected. Recalling that a sufficiently energetic molecule expands in the Morse potential (by Phase 1), and noting that the strictly decreasing upper PE surface V_2 clearly forces a molecule to expand, it follows that an overall molecular expansion is expected in this PE landscape. But since the coupling potential $V_{12}(X)$ diminishes with $X > 0$, and since the molecule expands with time, then coupling weakens with time. Therefore, we expect the amplitude of the ground state population to diminish, consistent with observation. The trend of the ground state population relates to the force expectation value. We observe that the force expectation value $\langle \hat{\mathbf{F}} \rangle$ oscillates with the frequency

as does the ground state population, and its amplitude also diminishes. However, the force attains a local maximum value only when the ground state population attains a local minimum value, and vice versa (Figure 5). This reflects an opposition between the lower and upper PE surfaces; since the lower PE surface $V_1(X)$ produces a negative force (for $X > 0$) while the upper PE surface $V_2(X)$ produces a positive force, an increase in the ground state population implies a decrease in the expected force, and vice versa. Finally, as the molecule expands, the slopes of both PE surfaces as well as the coupling potential tend to 0, and this explains the diminishing amplitude of the expected force.

The general trend of the ground state population observed in Case 1 (i.e., damped oscillation) is also observed in Cases 2–7. We are therefore primarily concerned with three parameters that largely characterize the trend of the ground state population \mathbf{G} : 1) the first maximum (or initial amplitude) G_A of \mathbf{G} , 2) the frequency (or inverse period) G_ν of \mathbf{G} , and 3) the asymptotic limit G_L of \mathbf{G} . We proceed to examine the effect of each of the five model parameters on the ground state population.

The first parameter (A) is the dissociation energy in the Morse potential V_1 . Increasing A from 5 to 10 to 15 has little to no effect on the dynamics of the ground state population (the cases $A = 5$ and $A = 15$ are not listed in Table 1). That is, all three cases are equivalent to the standard case. Therefore, \mathbf{G} is not sensitive to varying A on $[5, 15]$. We expect that the dissociation energy becomes significant only once the molecule expands to a considerable size. But recall that in the single-state case, little expansion occurs on the time interval $[0, 6]$ (By Phase 1, Figures 4a and 4d). Hence, the weak dependence of \mathbf{G} on A suggests that the ground state population

varies on a time scale much smaller than the time for molecular dissociation (Compare the time scales used in Phase 1 vs Phase 2, i.e., $[0, 50]$ vs $[0, 6]$).

The second parameter (B) directly modulates the vertical off-set of the upper PE surface V_2 . We observe that if B is increased, then the frequency G_ν of \mathbf{G} increases but the initial amplitude G_A and asymptotic limit G_L both decrease (Figures 5a and 6). Since G_A and G_L decrease, we conclude that raising the upper PE surface leads to weaker coupling and hence to a less efficient electronic de-excitation. In other words, to facilitate a strong de-excitation, a low upper PE surface is preferred.

The third parameter (C) is the central maximum of the Gaussian coupling potential V_{12} . We observe that if C is increased, then all three of G_A , G_ν , and G_L increase (Figures 5a and 7). Clearly then, given that a molecule is initially excited, a stronger coupling potential leads to a stronger and more effective electronic de-excitation. In particular, the asymptotic ground state population G_L gets closer to 50% (equilibrium between the two states) as C is increased. The observed effect of C is also consistent with the effect of B in the following sense: It is possible that raising the upper PE surface effectively lowers the coupling potential (i.e., V_2 and V_{12} “compete” with each other in the diabatic Schrödinger Equation). If this is the case, then it clearly follows that raising the upper PE surface weakens coupling and hence de-excitation.

The fourth parameter (D) controls the width of the Gaussian coupling potential V_{12} ; a greater value of D produces a narrower coupling potential. We observe that if D is increased, then G_A and G_ν both decrease. Moreover, the rate at which the amplitude diminishes increases (Figures 5a and 8). The last observation is consistent with expectation; as the molecule expands with time, the coupling potential dimin-

ishes. Clearly, a narrower coupling potential diminishes more rapidly. Finally, notice that G_L increases if D is increased from 0.1 (Figure 5a) to 1 (Figure 8b). Expecting that $G_L \rightarrow 0$ as $D \rightarrow \infty$ (since the coupling potential vanishes), it follows that there exists a value of D for which G_L is locally maximum. Thus, the width of the coupling potential is critical in optimizing de-excitation.

The fifth and final parameter (E) is the location at which the coupling potential is centered.

In Case 1 (the standard case), the coupling potential is centered at the equilibrium configuration ($E = 0$). We observe that if the coupling potential is displaced by 5 units in either direction ($E = \pm 5$), then G_A , G_ν , and G_L all decrease dramatically compared to $E = 0$. Further, the amplitude of oscillation is no longer strictly decreasing (Figure 5a and 9). This reflects the narrowness of the initial Gaussian wave function. Using $E = \pm 5$, the coupling potential $V_{12}(0)$ at $X = 0$ is too small to facilitate a strong state transition while the wave function is still near $X = 0$. Since the molecule expands (i.e., $\langle X \rangle$ increases), we expect that the coupling potential centered at $E = 5$ will be effective once the wave function reaches it. But surprisingly, the coupling potential is no more effective at $E = 5$ than it is at $E = -5$. On the contrary, the frequency G_ν is less at $E = 5$ than it is at $E = -5$ (Figure 9). This may reflect either the slow expansion of the molecule or possibly even the dispersion of the wave function as it evolves.

3.3 The Two-Dimensional Two-State Case

In Phase 3, we consider a molecule that can both stretch and twist. Thus, the PE surfaces are two-dimensional. Recall that the initial wave packet is given by Equation (28) and the PE functions are given by Equations (29)–(31):

$$\chi_1(X, \theta, 0) = 0$$

$$\chi_2(X, \theta, 0) = e^{-5(X-X_0)^2 - 5(|\theta - \theta_0 + \pi| - \pi)^2}$$

$$V_1(X, \theta) = 0.1X^2 + 5(1 - \cos \theta)$$

$$V_2(X, \theta) = 0.1X^2 + 10 - 5(1 - \cos \theta)$$

$$V_{12}(X, \theta) = X,$$

where X_0, θ_0 are model parameters. We use the interval $[X_1, X_2] \times [\theta_1, \theta_2] = [-10, 10] \times [-\pi, \pi]$ with space step size $\Delta X = 0.002\pi$ and time step size $\Delta t = 0.005$. We consider four cases, i.e., we consider four configurations (X_0, θ_0) at which the initial Gaussian wave packet can be centered. For each, we study the dynamics of the molecule in terms of absolute torsion angle, ground state population, and torque. The model parameter values used for each case are listed in Table 2.

| Case | X_0 | θ_0 |
|------|-------|-----------------|
| 1 | 0 | 0 |
| 2 | 0 | $\frac{\pi}{2}$ |
| 3 | 0 | π |
| 4 | 10 | $\frac{\pi}{2}$ |

Table 2: List of the model parameter values used for each case in Phase 3.

In Cases 1–3, the molecule is on average neither stretched nor compressed along

its torsion axis ($X_0 = 0$). In Case 1, the molecule is initially in the cis configuration ($\theta_0 = 0$). But since the molecule is initially excited (i.e., on the upper PE surface), it is unstable in the cis configuration. As time passes, we observe that $\hat{\theta}$ increases; i.e., the molecule twists away from the cis configuration and towards the trans configuration. Eventually, $\hat{\theta}$ fluctuates about $\theta \approx \frac{\pi}{2}$, suggesting that the molecule settles into an average state that does not strongly prefer either the cis configuration or the trans configuration over the other (Figure 10a). The angular motion of the molecule relates to the trend of the ground state population. As time passes, the ground state population increases and then fluctuates near $\mathbf{G} = 0.45$ (Figure 10b). Since the lower PE surface forces the molecule towards the cis configuration while the upper PE surface forces the molecule towards the trans configuration, a ground state population of $\mathbf{G} = 0.45$ is consistent with the observation that the molecule is not significantly more inclined towards either the cis or trans configurations. The trend of the torque expectation value is consistent with that of the ground state population, and this is analogous to the relationship between the force expectation value and ground state population in the one-dimensional case. That is, $\hat{\tau}$ attains a local maximum value only when \mathbf{G} attains a locally minimum value, and vice versa. This reflects the opposition of the two PE surfaces, in the sense that the lower PE surface produces a negative torque, while the upper PE surface produces a positive torque. Overall, $\hat{\tau}$ decreases and converges towards a positive value (Figure 10c). This is consistent with the increase of \mathbf{G} and the ultimate value $\mathbf{G} = 0.45 < 0.5$ (i.e., more of the wave function follows the upper PE surface).

In Case 2, the molecule is initially half-way between the pure cis and trans con-

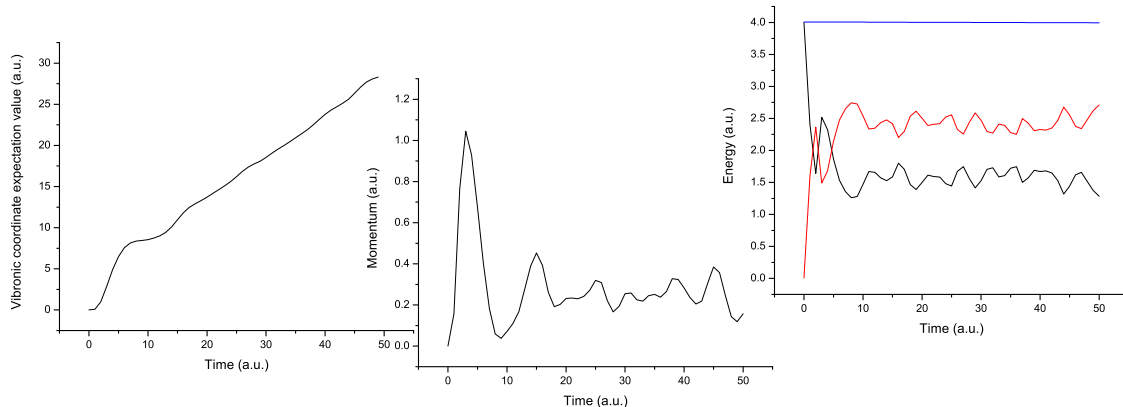
configurations ($\theta_0 = \frac{\pi}{2}$). But since the molecule is initially excited, it initially prefers the trans configuration. Note that the initial configuration of the molecule is also a point of electronic degeneracy. As time passes, $\hat{\theta}$ fluctuates roughly about $\theta = \frac{\pi}{2}$ (Figure 11a). This is similar to the eventual trend of $\hat{\theta}$ in Case 1 (Figure 10a). However, at time $t = 0.5$, the maximum torsion angle in Case 2 ($\hat{\theta} = 1.85$) exceeds the maximum torsion angle in Case 1 ($\hat{\theta} = 1.7$). This is a consequence of the bias of the initial molecule to the trans configuration on the upper PE surface. Eventually, however, the molecule is not strongly biased to either the cis or trans configurations. This is consistent with the trends of both the ground state population (Figure 11b) and of the torque expectation value (Figure 11c). We observe that the ground state population exhibits fluctuations that are not present in Case 1. This suggests an increased coupling action in some sense near the point of electronic degeneracy. Recalling from the one-dimensional case that an efficient electronic de-excitation requires a low upper PE surface and analogously that an efficient electronic excitation requires a low lower PE surface, it follows that an efficient de-excitation occurs to the right of the point of electronic degeneracy and that an efficient excitation occurs to the left. This explains the fluctuations we see about $\theta = \frac{\pi}{2}$. Nevertheless, it is interesting that the contrast between Case 1 and Case 2 is not dramatic. It therefore seems that fast transitions that supposedly occur at points of electronic degeneracy cannot be observed in the diabatic frame.

In Case 3, the molecule is initially in the trans configuration ($\theta_0 = \pi$). Since the molecule is excited, it is stable in the trans configuration. But despite its stability, the molecule exhibits very interesting dynamics. As time begins to pass, the ground

state population begins to increase (Figure 12b). But in the ground state, the trans configuration is unstable. Therefore, the molecule begins to transition from a stable state to an unstable state. Moreover, as time passes, the ground state population fluctuates but maintains an overall increasing trend. The ground state population eventually reaches $\mathbf{G} \approx 0.6 > 0.5$ (Figure 12b). This is in sharp contrast with Cases 1 and 2. This supports the recurring idea that molecular de-excitation is most effective at a configuration where the upper PE surface takes a low value. Notice further that at the configuration $(X, \theta) = (0, \pi)$, the lower PE surface attains its global maximum ($V_1 = 10$) and the upper PE surface attains its global minimum ($V_2 = 0$). We therefore conclude that a state transition is most effective when transitioning from a PE minimum (i.e., stable equilibrium) on one surface to a PE maximum (i.e., unstable equilibrium) on another surface. Since we are ultimately more likely to observe the molecule in the ground state ($\mathbf{G} \approx 0.6$) and since the lower PE surface forces the molecule to move towards the cis configuration, it is reasonable to observe that the torsion angle $\hat{\theta}$ eventually leans closer toward the cis configuration; we observe that $\hat{\theta}$ attains a minimum of $\hat{\theta} \approx 1$ (Figure 12a). Further, it is also reasonable that the expected torque on the molecule is ultimately negative ($\hat{\tau} \approx -0.5$), since the molecule ultimately prefers the cis configuration (Figure 12c).

In Case 4, the molecule is initially stretched ($X_0 = 10$) and is between the cis and trans configurations ($\theta_0 = \frac{\pi}{2}$). Since the molecule is stretched, the action of the coupling potential is much more significant. Since the molecule is initially excited, it initially prefers the trans configuration. This explains the slight bias of the expected torsion angle towards the trans configuration (Figure 13a). As time passes, the ground

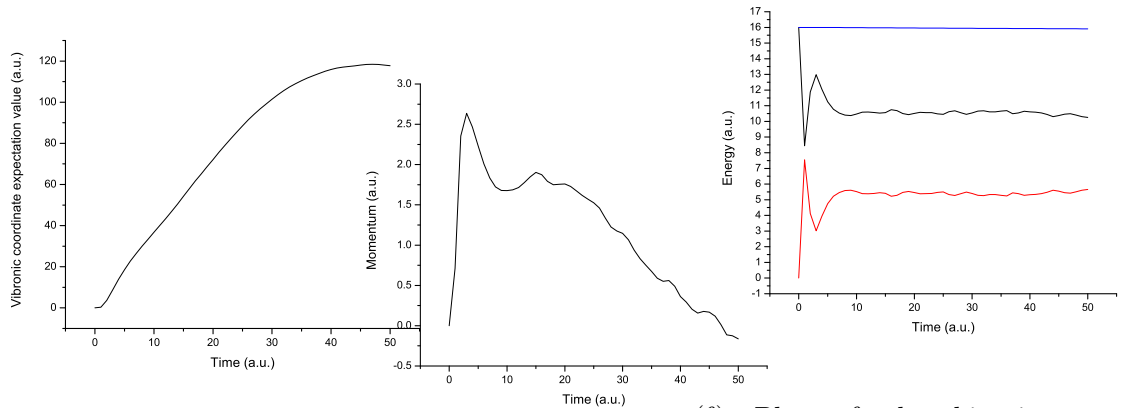
state population exhibits a trend like that generally seen in the one-dimensional case; the ground state population oscillates with an amplitude that diminishes and leads to the asymptotic limit $\mathbf{G} \approx 0.5$ (Figure 13b). That is, the molecule prefers neither the cis nor the trans configuration. The rapid decay of the amplitude reflects the weakening of the coupling potential as the molecule relaxes from its stretched configuration. The expected torque is consistent with the ground state population as in previous cases. We observe that the torque diminishes and vanishes with time (Figure 13c), which is consistent with the asymptotic limit $G_L = 0.5$. Case 4 reminds us that in addition to the right shapes for the two PE surfaces, a strong coupling potential is also essential for an effective state transition.



(a) Plot of the vibronic coordinate expectation value against time for Case 1 ($A = 4$).

(b) Plot of the momentum expectation value against time for Case 1 ($A = 4$).

(c) Plot of the kinetic potential expectation values against time for Case 1 ($A = 4$).

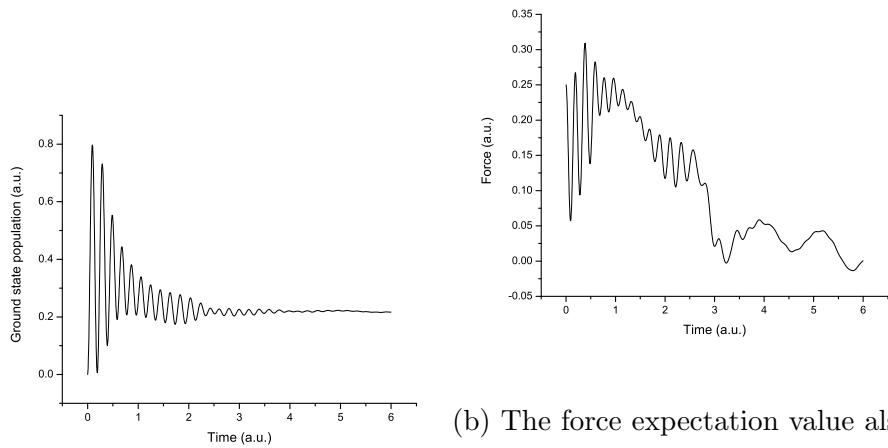


(d) Plot of the vibronic coordinate expectation value against time for Case 2 ($A = 16$).

(e) Plot of the momentum expectation value against time for Case 2 ($A = 16$).

(f) Plot of the kinetic potential expectation values against time for Case 2 ($A = 16$).

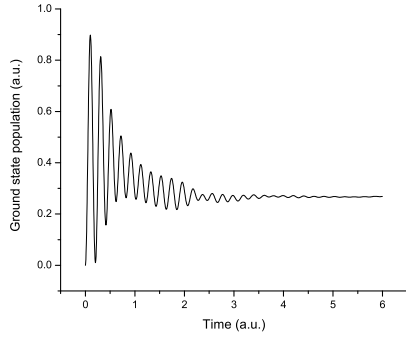
Figure 4: Plots of expectation values for both cases considered in Phase 1.



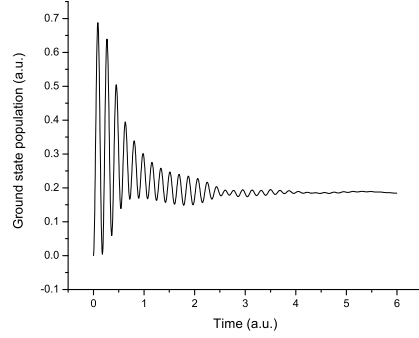
(a) The ground state population oscillates with time, with diminishing amplitude.

(b) The force expectation value also oscillates like the ground state population, except that its minima occur where the maxima of the ground state population occur, and vice versa.

Figure 5: Plots of the ground state population and the force expectation value against time for Case 1 (the standard case) in Phase 2.

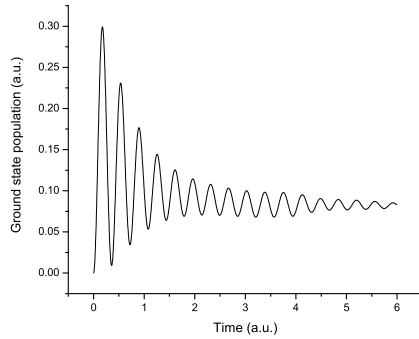


(a) For Case 2 ($B = 15 < 20$).

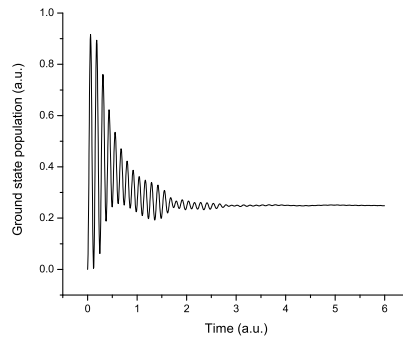


(b) For Case 3 ($B = 25 > 20$).

Figure 6: Plots of the ground state population against time for two different values of the parameter B in Phase 2. The standard value is $B = 20$ used in Case 1 (Figure (4a)).

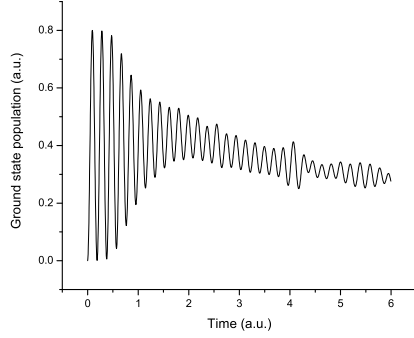


(a) For Case 4 ($C = 5 < 15$).

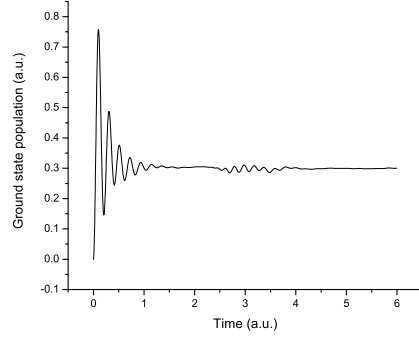


(b) For Case 5 ($C = 25 > 15$).

Figure 7: Plots of the ground state population against time for two different values of the parameter C in Phase 2. The standard value is $C = 15$ used in Case 1 (Figure (4a)).

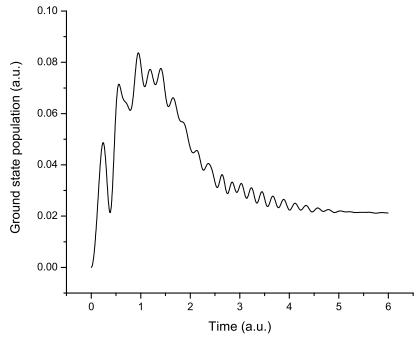


(a) For Case 6 ($D = 0.01 < 0.1$).

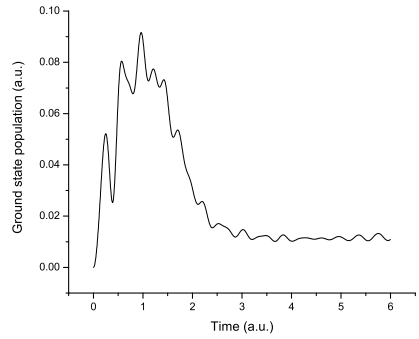


(b) For Case 7 ($D = 1 > 0.1$).

Figure 8: Plots of the ground state population against time for two different values of the parameter D in Phase 2. The standard value is $D = 0.1$ used in Case 1 (Figure (4a)).

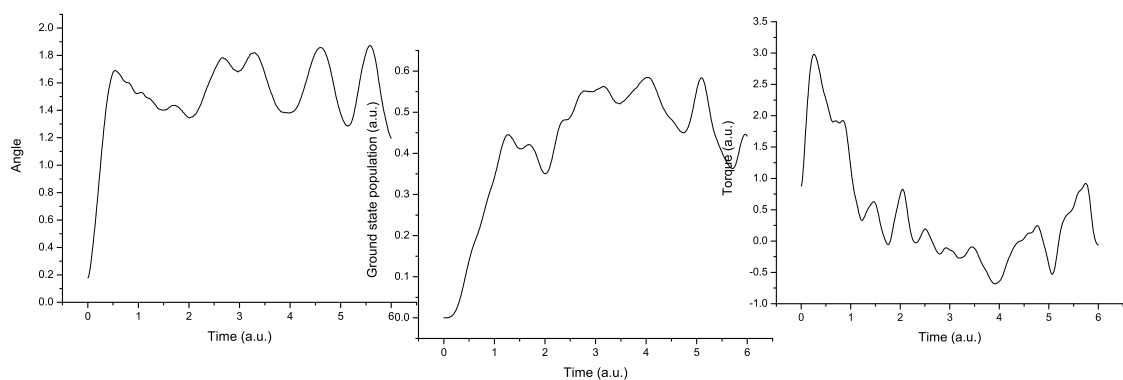


(a) For Case 8 ($BE = -5 < 0$).



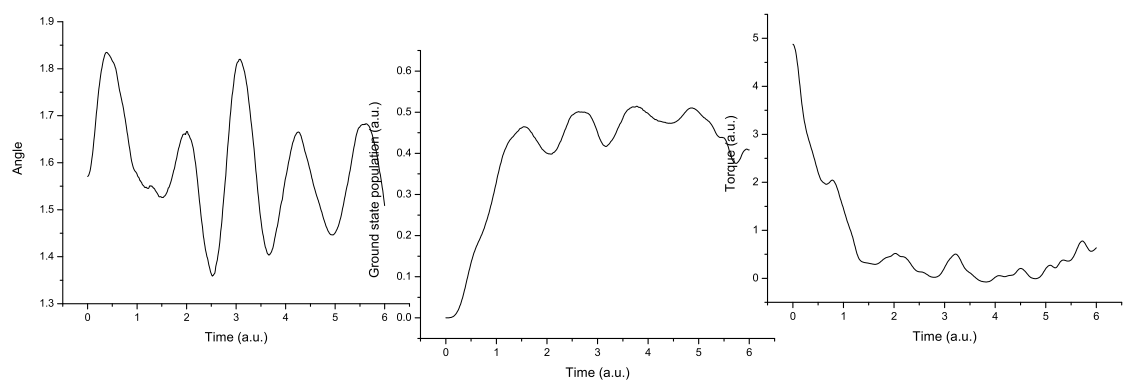
(b) For Case 9 ($E = 5 > 0$).

Figure 9: Plots of the ground state population against time for two different values of the parameter E in Phase 2. The standard value is $E = 0$ used in Case 1 (Figure (4a)).



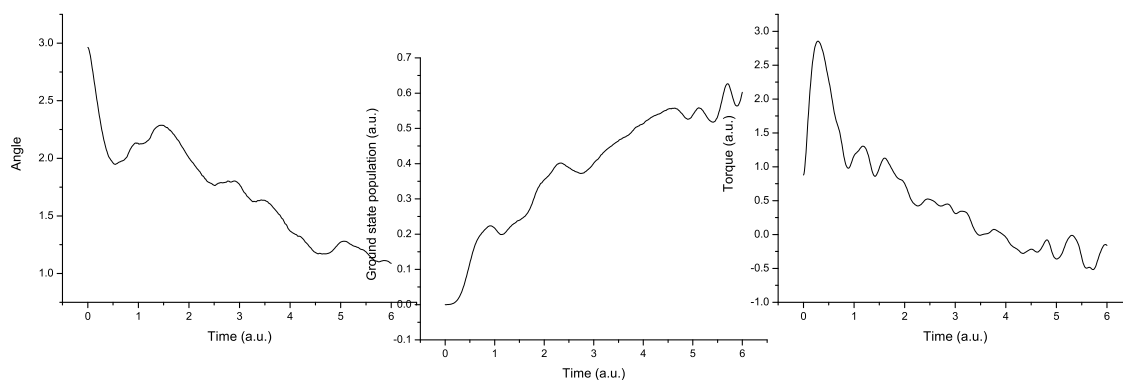
- (a) Plot of the absolute torsion angle expectation value $\hat{\theta}$ against time.
- (b) Plot of the ground state population \mathbf{G} against time.
- (c) Plot of the torque expectation value $\hat{\tau}$ against time.

Figure 10: Plots of the torsion angle, ground state population, and torque for a molecule in Case 1 of Phase 3.



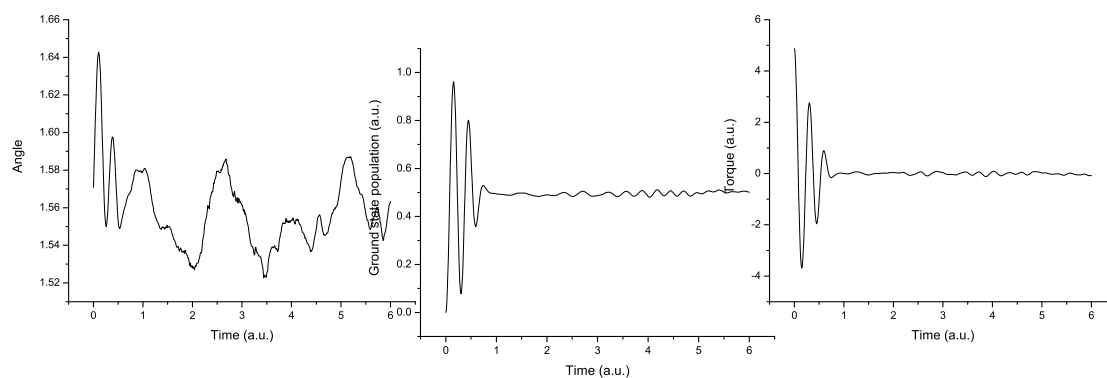
(a) Plot of the absolute torsion angle expectation value $\hat{\theta}$ against time. (b) Plot of the ground state population \mathbf{G} against time. (c) Plot of the torque expectation value $\hat{\tau}$ against time.

Figure 11: Plots of the torsion angle, ground state population, and torque for a molecule in Case 2 of Phase 3.



- (a) Plot of the absolute torsion angle expectation value $\hat{\theta}$ against time.
- (b) Plot of the ground state population \mathbf{G} against time.
- (c) Plot of the torque expectation value $\hat{\tau}$ against time.

Figure 12: Plots of the torsion angle, ground state population, and torque for a molecule in Case 3 of Phase 3.



(a) Plot of the absolute torsion angle expectation value $\hat{\theta}$ against time. (b) Plot of the ground state population \mathbf{G} against time. (c) Plot of the torque expectation value $\hat{\tau}$ against time.

Figure 13: Plots of the torsion angle, ground state population, and torque for a molecule in Case 4 of Phase 3.

4 Discussion

In principle, the evolution of a molecule can be treated as a quantum-mechanical many-body problem. But such a treatment is not practical. Instead, we cast the molecular wave function in either one of the adiabatic or nonadiabatic (i.e., diabatic) frames. Both frames allow for a simpler study of the two fundamental aspects of a molecule as it evolves—its nuclear and electronic configurations. The nuclear wave function encodes the nuclear configuration and electronic state in which we can expect to observe the molecule. We were interested in understanding the relationship between the nuclear and electronic configurations—How does the probability of a state transition depend on the molecular structure? In particular, we were interested in the dynamics of the ground state population for an initially excited molecule. We studied the dependence of these dynamics on the PE landscape in the diabatic frame.

We constructed a numerical model for the evolution of the nuclear wave function in the diabatic frame. For a single-state one-dimensional landscape (Phase 1), the evolution scheme takes the form of a simple tridiagonal system that is solved recursively. For a two-state landscape (Phase 2) and a two-dimensional landscape (Phase 3), we extended our model using the ADI method. This method allowed us to preserve the recursive and tridiagonal structure of our evolution scheme. In this way, our model remains very simple and takes complete advantage of matrix sparseness. In each phase of the study, we analyzed the numerical predictions of our model and concluded that they were physically meaningful. Therefore, the numerical scheme that we outlined carries the potential to describe trends and relationships existent in real physical systems.

There are a number of results that deserve further exposition and discussion. First, we recall the result from Phase 2 that there exists a width of the coupling potential for which the ultimate ground state population assumes a local minimum. Since we expect the ultimate ground state population to vanish as the coupling potential width vanishes, we reasoned that there exists a coupling potential width for which the ultimate ground state population assumes a local maximum. That is, in general terms, it is possible for a molecule to have a PE landscape whose geometry guarantees a greater ground state population limit during de-excitation, as compared to other very similar PE landscapes. This is significant because it supports the idea that biological molecules have PE landscapes whose geometries locally optimize overall de-excitation for the purposes of maintaining homeostasis.

Second, we recall the result from Phase 2 that the ground state population of a diatomic molecule depends weakly on the dissociation energy of the lower PE surface. We explained this with the observation that the dynamics of the ground state population for a diatomic molecule occur on a time scale much smaller than that for molecular dissociation. However, we saw that both the frequency of oscillation and over all decay rate of the ground state population vary with the shape of the PE landscape. In particular, given sufficiently weak but broad coupling, it may be possible to have the ground state population vary on a time scale comparable to that for molecular expansion. In this case, the dissociation energy may become significant. Here, we recall a result from Phase 3 whose interpretation suggests that raising the lower PE surface boosts the ultimate ground state population. If this holds for the diatomic molecule in Phase 2, then it follows that raising the dissociation energy of the

lower PE surface will increase the ultimate ground state population. In other words, under sufficiently weak and broad coupling, a strongly bound diatomic molecule is more likely to be in the ground state than is a more weakly bound molecule with the same initial conditions.

Third, we recall the result from Phase 3 that in the diabatic frame, the transition to the ground state population during cis-trans isomerization is not faster at the point of electronic degeneracy $\theta = \frac{\pi}{2}$. We had concluded that the diabatic frame is incapable of detecting fast transitions at such points. However, it may be possible to explain why this is the case: Since the adiabatic and diabatic frames are complete orthonormal basis sets, there exists a unitary transformation mapping one frame onto the other. Assuming that the basis sets are real-valued, the unitary transformation from the diabatic frame to the adiabatic frame is a rotation matrix W given by the tensor product of the basis sets:

$$W(\mathbf{X}) = \begin{bmatrix} \langle \psi_1(\mathbf{x}, \mathbf{X}) | \phi_1(\mathbf{x}) \rangle & \langle \psi_1(\mathbf{x}, \mathbf{X}) | \phi_2(\mathbf{x}) \rangle \\ \langle \psi_2(\mathbf{x}, \mathbf{X}) | \phi_1(\mathbf{x}) \rangle & \langle \psi_2(\mathbf{x}, \mathbf{X}) | \phi_2(\mathbf{x}) \rangle \end{bmatrix},$$

where the brackets are taken over \mathbf{x} . Note that $W(\mathbf{X}^0)$ is the identity matrix. If \mathbf{X}^0 is chosen to be the point of electronic degeneracy, then we expect the transformation from the diabatic frame into the adiabatic frame at a configuration \mathbf{X} far from \mathbf{X}^0 to be nontrivial. Given that Cases 1 and 2 in Phase 3 have very similar ground state populations in the diabatic frame, the nontrivial rotational transformation into the adiabatic frame by W for both Case 1 and Case 2 implies that the ground state populations in the two cases will be different. In other words, the observation that Cases 1 and 2 are similar in the diabatic frame may, in fact, be an indication that Cases 1 and 2 are very dissimilar in the adiabatic frame. This opens the possibility

that the results we obtained in Phase 3 are indirectly reflecting the occurrence of a fast transition at the point of electronic degeneracy in the adiabatic frame.

Fourth and finally, we recall the result from Phase 3 that the transition to the ground state was most effective at the nuclear configuration where the lower PE surface attains its maximum value and the upper PE surface attains its minimum value. Thus, although we did not observe a fast transition at the point of electronic degeneracy in the diabatic frame, there is another special configuration at which we did observe a fast transition (Case 3 in Phase 3). This is a very important conclusion because it reveals a feature common to the adiabatic and diabatic frames. In both frames, a fast electronic transition from one PE surface to another is most effective at a nuclear configuration that is stable and minimally energetic on the first PE surface but that is unstable and highly energetic on the second PE surface. In the case of the adiabatic frame, it turns out that these special configurations are precisely the points of electronic degeneracy. But as we observed, this is not the case in the diabatic frame. Despite the common fundamental feature that the two frames share, the frames still differ in some respect. This difference, however, seems to be the result of a more fundamental difference between the geometries of the adiabatic PE landscape and diabatic PE landscape. In the adiabatic PE landscape, the upper PE surface is never below the lower PE surface ($V_1^A(\mathbf{X}) \leq V_2^A(\mathbf{X})$ for all \mathbf{X}). This simply follows from the definitions of ground state energy and excited state energy. Consequently, in the adiabatic frame, a nuclear configuration at which the lower PE surface is maximum and the upper PE surface is a minimum is at best a tangential intersection point of the two surfaces, i.e., a point of electronic degeneracy. In contrast, if we transform

the adiabatic PE landscape into the diabatic frame (by applying $W^{-1}(\mathbf{X})$), then in the resulting diabatic PE landscape, it is possible for the upper PE surface to fall below the lower PE surface at some configurations ($V_1^D(\mathbf{X}) > V_2^D(\mathbf{X})$ for some \mathbf{X}). This was indeed the case for the diabatic PE landscape used in Phase 3. In this case, the lower PE surface is not necessarily at its maximum (or the upper PE surface is not necessarily at its minimum) at the intersection points between the two PE surfaces. That is, in the diabatic PE landscape, an intersection point is not necessarily tangential. It follows that in the diabatic frame, fast transitions do not necessarily occur at points of electronic degeneracy but might instead occur at some other special nuclear configuration, just as we observed in Phase 3.

Mathematically, the efficiency of a transition is determined by the competition of the PE surfaces with the coupling term in the Schrödinger Equation. From a purely mathematical perspective, electronic degeneracy plays no role in the efficiency of state transitions per se. Electronic degeneracy is important only in the context of physics. That is, since the adiabatic frame is “physically more meaningful” than its diabatic counterpart, and since fast transitions occur at points of electronic degeneracy in the adiabatic frame, we can say that electronic degeneracy is important for fast transitions in the context of physics. Our study simply provides the insight that this is not mathematically necessary. In conclusion, our numerical model allowed us to study basic molecular dynamics in the diabatic frame, and in our study we learned that the adiabatic and diabatic frames are in some ways mathematically similar but physically different.

5 Future Work

We would like to extend our numerical model to the case of a molecule with three nuclear degrees of freedom. We would also like to numerically construct the unitary transformation from the diabatic frame into the adiabatic frame. This would allow us to transform our results into the adiabatic frame, and it would be interesting to interpret the dynamics of the ground state population in the adiabatic setting. Finally, we would like to study the effects of an artificial “sink” for kinetic energy in the ground state. Such a sink would influence the system to prefer the ground state. This could possibly model the mechanism for fast homeostatic de-excitations in large biomolecular complexes.

BIBLIOGRAPHY

- [1] Hagelberg, Frank. *Electron Dynamics in Molecular Interactions*. Imperial College Press: London, 2014.
- [2] Lösch, Wolfgang. *Numerical Solution of the Time-Dependent Schrödinger Equation*. <http://www.heineshof.de>. 2011.
- [3] Flannery, B.P.; Press, W.H.; Teukolsky, S.A.; Vetterling, W.T. *Numerical Recipes: The Art of Scientific Computing*. Cambridge University Press: New York, 1989.